

# 2 Quantum Tomographic Methods

Giacomo Mauro D'Ariano<sup>1</sup>, Matteo G.A. Paris<sup>2</sup>, and  
Massimiliano F. Sacchi<sup>1</sup>

<sup>1</sup> Unità INFN and Dipartimento di Fisica "A. Volta", Università di Pavia, Italia

<sup>2</sup> Unità INFN and Dipartimento di Fisica, Università di Milano, Italia

**Abstract.** The state of a physical system is the mathematical object that provides a complete information on the system. The knowledge of the state is equivalent to know the result of any possible measurement on the system. This chapter reviews quantum state estimation for a generic quantum system by quantum tomography i.e. from the measurement of a suitable set of observables, a quorum, on repeated preparations of the system. Topics include characterization of quora, determination of the expectation value of any operator (including the nondiagonal projectors needed to construct a matrix representation of the density operator), evaluation of pattern functions, effect of instrumental noise, and example of tomographic procedure for harmonic systems and spins.

## 2.1 Introduction

The state of a physical system is any mathematical object that provides a complete information on the system. The knowledge of the state is equivalent to know the result of any possible measurement on the system. In Classical Mechanics the state of a system, say a particle, is specified by the set of canonical coordinates and, at least in principle, it is always possible to devise a procedure made of multiple measurements which fully recovers the state. In Quantum Mechanics, on the contrary, this is not possible, due to the fundamental limitations related to the Heisenberg uncertainty principle [1, 2] and the no-cloning theorem [3]. In fact, on one hand one cannot perform an arbitrary sequence of measurements on a single system without inducing on it a back-action of some sort. On the other hand, it is not possible to create a perfect copy of the system without already knowing its state in advance. Thus, there is no way out, not even in principle, to infer the quantum state of a single system without having some prior knowledge on it [4]. For a quantum mechanical system it is possible to estimate the unknown state of a system when many identical copies are available in the same state, so that a different measurement can be performed on each copy. A procedure of this kind is called *quantum tomography*. The problem of finding a procedure to determine the state of a system from multiple copies was first addressed in 1957 by Fano [5], who called *quorum* a set of observables sufficient for a complete determination of the density matrix. However, since for a particle it is difficult to devise concretely measurable observables other than position,

momentum and energy, the fundamental problem of measuring the quantum state has remained at the level of mere speculation up to almost ten years ago, when the issue finally entered the realm of experiments with the pioneering experiments by Raymer’s group [6] in the domain of quantum optics. In quantum optics, in fact, using a balanced homodyne detector one has the unique opportunity of measuring all possible linear combinations of position and momentum of a harmonic oscillator representing a single mode of the electromagnetic field.

The first technique to estimate the elements of the density operator from homodyne measurements — so called *homodyne tomography* — originated from the observation by Vogel and Risken [7] that the collection of probability distributions achieved by homodyne detection is just the Radon transform of the Wigner function  $W$ . Therefore, as in classical imaging, by Radon transform inversion one can obtain  $W$ , and then from  $W$  the matrix elements of the density operator. This first method, however, was affected by uncontrollable approximations, since arbitrary smoothing parameters are needed for the inverse Radon transform. In [8] the first exact technique was given for measuring experimentally the matrix elements of the density operator in the photon-number representation, by simply averaging functions of homodyne data. After that, the method was further simplified [9], and the feasibility for non-unit quantum efficiency of detectors—above some bounds—was established.

The exact homodyne method has been implemented experimentally to measure the photon statistics of a semiconductor laser [10], and the density matrix of a squeezed vacuum [11]. The success of optical homodyne tomography has then stimulated the development of state-reconstruction procedures for atomic beams [12], the experimental determination of the vibrational state of a molecule [13], of an ensemble of helium atoms [14], and of a single ion in a Paul trap [15].

Using quantum tomography the state is perfectly recovered in the limit of infinite number of measurements, while in the practical finite-measurements case, one can always estimate the statistical error that affects the reconstruction. For infinite dimensions the propagation of statistical errors of the density matrix elements make them useless for estimating the ensemble average of unbounded operators, and a method for estimating the ensemble average of arbitrary observable of the field without using the density matrix elements has been derived [16]. Further insights on the general method of state reconstruction has led to generalize homodyne tomography to any number of modes [17], and then to extend the tomographic method from the harmonic oscillator to an arbitrary quantum system using group theory [18–21]. A general data analysis method has been designed in order to unbiased the estimation procedure from any known instrumental noise [20]. Moreover, algorithms have been engineered to improve the statistical errors on a given sample of experimental data—the so-called adaptive tomography [22]—and then maximum-likelihood strategies [23] have been used that improved dramatically statis-

tical errors, however, at the expense of some bias in the infinite dimensional case, and of exponential complexity versus  $N$  for the joint tomography of  $N$  quantum systems. Quantum tomographic methods to perform fundamental tests of quantum mechanics have been proposed, as the measure of the non-classicality of radiation field of [24], and the test of the state reduction rule using light from parametric downconversion of [25].

The latest technical developments [26] derive the general tomographic method from spanning sets of operators, the previous group theoretical approaches [18–21] being just a particular case of this general method, where the group representation is just a device to find suitable operator “orthogonality” and “completeness” relations in the linear algebra of operators. Finally, very recently, a method for tomographic estimation of the unknown quantum operation of a quantum device has been derived [27], which uses a single fixed input entangled state, which plays the role of all possible input states in quantum parallel on the tested device, making finally the method a true “quantum radiography” of the functioning of a device.

This chapter is structured to give a self-contained and unified derivation of the methods of quantum tomography. In Sect. 2 we introduce the generalized Wigner functions [28, 29] while in Sect. 3 we provide the basic elements of detection theory in quantum optics: photodetection, homodyne detection, and heterodyne detection. As we will see, heterodyne detection also provides a method for estimating the ensemble average of polynomials in the field operators, however, it is unsuitable for the density matrix elements in the photon-number representation. The effect of non unit quantum efficiency is taken into account for all such detection schemes. In Sect. 4 we give a brief history of quantum tomography, starting with the first proposal of Vogel and Risken [7] as the extension to the domain of quantum optics of the conventional tomographic imaging. As already mentioned, this method indirectly recovers the state of the system through the reconstruction of the Wigner function, and is affected by uncontrollable bias. The exact homodyne tomography method of [8] (successively simplified in [9]) is here presented on the basis of the general tomographic method of spanning sets of operators of [26]. As another application of the general method, the tomography of spin systems [30] is provided from the group theoretical method of [18–20]. In this section we also include further developments to improve the method, such as the deconvolution techniques of [20] to correct the effects of experimental noise by data processing, and the adaptive tomography [22] to reduce the statistical fluctuations of tomographic estimators. The generalization of [17] of homodyne tomography to many modes of radiation is reviewed in Sect. 5, where it is shown how tomography of a multimode field can be performed by using only a single local oscillator with a tunable field mode. Some results of Monte Carlo simulations from [17] are also shown for the state that describes light from parametric downconversion. Section 6 is devoted to reconstruction techniques [23] based on the maximum likelihood principle, which are suited to the estimation of a finite number of parameters, as proposed in [31], or

to the state determination in the presence of very low number of experimental data [23]. Unfortunately, the algorithm of this method has exponential complexity versus the number of quantum systems for a joint tomography of many systems.

## 2.2 Wigner Functions

Since Wigner’s pioneering work [28], generalized phase-space techniques have proved very useful in various branches of physics [33]. As a method to express the density operator in terms of  $c$ -number functions, the Wigner functions often lead to considerable simplification of the quantum equations of motion, as for example, for transforming master equations in operator form into more amenable Fokker-Planck differential equations (see, for example, [34]). Using the Wigner function one can express quantum-mechanical expectation values in form of averages over the complex plane (the classical phase-space), the Wigner function playing the role of a  $c$ -number quasi-probability distribution, which generally can also have negative values. More precisely, the original Wigner function allows to easily evaluate expectations of symmetrically ordered products of the field operators, corresponding to the Weyl’s quantization procedure [35]. However, with a slight change of the original definition, one defines generalized  $s$ -ordered Wigner function  $W_s(\alpha, \alpha^*)$ , as follows [29]

$$W_s(\alpha, \alpha^*) = \int_{\mathbb{C}} \frac{d^2\lambda}{\pi^2} e^{\alpha\lambda^* - \alpha^*\lambda + \frac{s}{2}|\lambda|^2} \text{Tr}[D(\lambda)\rho], \quad (2.1)$$

where  $\alpha^*$  denotes the complex conjugate of  $\alpha$ , the integral is performed on the complex plane with measure  $d^2\lambda = d\text{Re}\lambda d\text{Im}\lambda$ ,  $\rho$  represents the density operator, and

$$D(\alpha) \equiv \exp(\alpha a^\dagger - \alpha^* a) \quad (2.2)$$

denotes the displacement operator, where  $a$  and  $a^\dagger$  ( $[a, a^\dagger] = 1$ ) are the annihilation and creation operators of the field mode of interest. The Wigner function in (2.1) allows one to evaluate  $s$ -ordered expectation values of the field operators through the following relation

$$\text{Tr}[:(a^\dagger)^n a^m :_s \rho] = \int_{\mathbb{C}} d^2\alpha W_s(\alpha, \alpha^*) \alpha^{*n} \alpha^m. \quad (2.3)$$

The particular cases  $s = -1, 0, 1$  correspond to *anti-normal*, *symmetrical*, and *normal* ordering, respectively. In these cases the generalized Wigner function  $W_s(\alpha, \alpha^*)$  are usually denoted by the following symbols and names

$$\begin{array}{ll} \frac{1}{\pi} Q(\alpha, \alpha^*) & \text{for } s = -1 \text{ “}Q \text{ function”} \\ W(\alpha, \alpha^*) & \text{for } s = 0 \text{ (usual Wigner function)} \\ P(\alpha, \alpha^*) & \text{for } s = 1 \text{ “}P \text{ function”} \end{array} \quad (2.4)$$

For the normal ( $s = 1$ ) and anti-normal ( $s = -1$ ) orderings, the following simple relations with the density matrix are well known

$$Q(\alpha, \alpha^*) \equiv \langle \alpha | \rho | \alpha \rangle, \quad (2.5)$$

$$\rho = \int_{\mathbb{C}} d^2\alpha P(\alpha, \alpha^*) |\alpha\rangle\langle\alpha|, \quad (2.6)$$

where  $|\alpha\rangle$  denotes the customary coherent state  $|\alpha\rangle = D(\alpha)|0\rangle$ ,  $|0\rangle$  being the vacuum state of the field. Among the three particular representations (2.4), the  $Q$  function is positively definite and infinitely differentiable (it actually represents the probability distribution for ideal joint measurements of position and momentum of the harmonic oscillator: see Sect. 2.3.3). On the other hand, the  $P$  function is known to be possibly highly singular, and the only pure states for which it is positive are the coherent states [36]. Finally, the usual Wigner function has the remarkable property of providing the probability distribution of the quadratures of the field in the form of a marginal distribution, namely

$$\int_{-\infty}^{\infty} d\text{Im}\alpha W(\alpha e^{i\varphi}, \alpha^* e^{-i\varphi}) = {}_{\varphi}\langle \text{Re}\alpha | \rho | \text{Re}\alpha \rangle_{\varphi}, \quad (2.7)$$

where  $|x\rangle_{\varphi}$  denotes the (unnormalizable) eigenstate of the field quadrature

$$X_{\varphi} = \frac{a^{\dagger} e^{i\varphi} + a e^{-i\varphi}}{2} \quad (2.8)$$

with real eigenvalue  $x$ . Notice that any couple of quadratures  $X_{\varphi}$ ,  $X_{\varphi+\pi/2}$  is canonically conjugate, namely  $[X_{\varphi}, X_{\varphi+\pi/2}] = i/2$ , and it is equivalent to position and momentum of a harmonic oscillator. Usually, negative values of the Wigner function are viewed as signature of a non-classical state, the most eloquent example being the Schrödinger-cat state [37], whose Wigner function is characterized by rapid oscillations around the origin of the complex plane. From (2.1) one can notice that all  $s$ -ordered Wigner functions are related to each other through Gaussian convolution

$$W_s(\alpha, \alpha^*) = \int_{\mathbb{C}} d^2\beta W_{s'}(\beta, \beta^*) \frac{2}{\pi(s' - s)} \exp\left(-\frac{2}{s' - s} |\alpha - \beta|^2\right) \quad (2.9)$$

$$= \exp\left(\frac{s' - s}{2} \frac{\partial^2}{\partial\alpha\partial\alpha^*}\right) W_{s'}(\alpha, \alpha^*), \quad (s' > s). \quad (2.10)$$

Equation (2.9) shows the positivity of the generalized Wigner function for  $s < -1$ , as a consequence of the positivity of the  $Q$  function. The maximum value of  $s$  keeping the generalized Wigner functions as positive can be considered as an indication of the classical nature of the physical state [38].

An equivalent expression for  $W_s(\alpha, \alpha^*)$  can be derived as follows [32]. Equation (2.1) can be rewritten as

$$W_s(\alpha, \alpha^*) = \text{Tr}[\rho D(\alpha) \hat{W}_s D^\dagger(\alpha)] , \quad (2.11)$$

where

$$\hat{W}_s = \int_{\mathbb{C}} \frac{d^2\lambda}{\pi^2} e^{\frac{s}{2}|\lambda|^2} D(\lambda) . \quad (2.12)$$

Through the customary Baker-Campbell-Hausdorff (BCH) formula

$$\exp A \exp B = \exp \left( A + B + \frac{1}{2}[A, B] \right) , \quad (2.13)$$

which holds when  $[A, [A, B]] = [B, [A, B]] = 0$ , one writes the displacement in normal order, and integrating on  $\arg(\lambda)$  and  $|\lambda|$  one obtains

$$\hat{W}_s = \frac{2}{\pi(1-s)} \sum_{n=0}^{\infty} \frac{1}{n!} \left( \frac{2}{s-1} \right)^n a^{\dagger n} a^n = \frac{2}{\pi(1-s)} \left( \frac{s+1}{s-1} \right)^{a^\dagger a} , \quad (2.14)$$

where we used the normal-ordered forms

$$:(a^\dagger a)^n: = (a^\dagger)^n a^n = a^\dagger a (a^\dagger a - 1) \dots (a^\dagger a - n + 1) , \quad (2.15)$$

and the identity

$$:e^{-x a^\dagger a}: = \sum_{l=0}^{\infty} \frac{(-x)^l}{l!} (a^\dagger)^l a^l = (1-x)^{a^\dagger a} . \quad (2.16)$$

The density matrix can be recovered from the generalized Wigner functions and, in particular, for  $s = 0$  one has the inverse of the Glauber formula

$$\rho = 2 \int_{\mathbb{C}} d^2\alpha W(\alpha, \alpha^*) D(2\alpha) (-)^{a^\dagger a} , \quad (2.17)$$

whereas for  $s = 1$  one recovers (2.6) that defines the  $P$  function.

### 2.3 Elements of Detection Theory

Here we evaluate the probability distribution of the photocurrent of photodetectors, balanced homodyne detectors, and heterodyne detectors. We show that under suitable limits the respective photocurrents provide the measurement of the photon number distribution, of the quadrature, and of the complex amplitude of a single mode of the electromagnetic field. When the effect of non-unit quantum efficiency is taken into account an additional noise affects the measurement, giving a Bernoulli convolution for photo-detection, and a Gaussian convolution for homodyne and heterodyne detection. Extensive use of the results in this section will be made in the context of quantum homodyne tomography.

### 2.3.1 Photodetection

Light is revealed by exploiting its interaction with atoms/molecules or electrons in a solid, and, essentially, each photon ionizes a single atom or promotes an electron to a conduction band, and the resulting charge is then amplified to produce a measurable pulse. In practice, however, available photodetectors are not ideally counting all photons, and their performance is limited by a non-unit quantum efficiency  $\zeta$ . In fact, only a fraction  $\zeta$  of the incoming photons lead to an electric signal, and ultimately to a *count*: some photons are either reflected from the surface of the detector, or are absorbed without being transformed into electric pulses.

Let us consider a light beam entering a photodetector of quantum efficiency  $\zeta$ , *i.e.* a detector that transforms just a fraction  $\zeta$  of the incoming light pulse into electric signal. If the detector is small with respect to the coherence length of radiation and its window is open for a time interval  $T$ , then the Poissonian process of counting gives a probability  $p(m; T)$  of revealing  $m$  photons that writes [39]

$$p(m; T) = \text{Tr} \left[ \rho : \frac{[\zeta I(T)T]^m}{m!} \exp[-\zeta I(T)T] : \right], \quad (2.18)$$

where  $\rho$  is the quantum state of light,  $: \cdot :$  denotes the normal ordering of field operators, and  $I(T)$  is the beam intensity

$$I(T) = \frac{2\epsilon_0 c}{T} \int_0^T \mathbf{E}^{(-)}(\mathbf{r}, t) \cdot \mathbf{E}^{(+)}(\mathbf{r}, t) dt, \quad (2.19)$$

given in terms of the positive (negative) frequency part of the electric field operator  $\mathbf{E}^{(+)}(\mathbf{r}, t)$  ( $\mathbf{E}^{(-)}(\mathbf{r}, t)$ ). The quantity  $p(t) = \zeta \text{Tr}[\rho I(T)]$  equals the probability of a single count during the time interval  $(t, t + dt)$ . Let us now focus our attention to the case of the radiation field excited in a stationary state of a single mode at frequency  $\omega$ . Equation (2.18) can be rewritten as

$$p_\eta(m) = \text{Tr} \left[ \rho : \frac{(\eta a^\dagger a)^m}{m!} \exp(-\eta a^\dagger a) : \right], \quad (2.20)$$

where the parameter  $\eta = \zeta c \hbar \omega / V$  denotes the overall *quantum efficiency* of the photodetector. Using (2.15) and (2.16) one obtains

$$p_\eta(m) = \sum_{n=m}^{\infty} \rho_{nn} \binom{n}{m} \eta^m (1 - \eta)^{n-m}, \quad (2.21)$$

where  $\rho_{nn} \equiv \langle n | \rho | n \rangle = p_{\eta=1}(n)$ . Hence, for unit quantum efficiency a photodetector measures the photon number distribution of the state, whereas for non unit quantum efficiency the output distribution of counts is given by a Bernoulli convolution of the ideal distribution.

The effects of non unit quantum efficiency on the statistics of a photodetector, *i.e.* (2.21) for the output distribution, can be also described by means of a simple model in which the realistic photodetector is replaced with an ideal photodetector preceded by a beam splitter of transmissivity  $\tau \equiv \eta$ . The reflected mode is absorbed, whereas the transmitted mode is photo-detected with unit quantum efficiency. In order to obtain the probability of measuring  $m$  clicks, notice that, apart from trivial phase changes, a beam splitter of transmissivity  $\tau$  affects the unitary transformation of fields

$$\begin{pmatrix} c \\ d \end{pmatrix} \equiv U_\tau^\dagger \begin{pmatrix} a \\ b \end{pmatrix} U_\tau = \begin{pmatrix} \sqrt{\tau} & -\sqrt{1-\tau} \\ \sqrt{1-\tau} & \sqrt{\tau} \end{pmatrix} \begin{pmatrix} a \\ b \end{pmatrix}, \quad (2.22)$$

where all field modes are considered at the same frequency. Hence, the output mode  $c$  hitting the detector is given by the linear combination

$$c = \sqrt{\tau}a - \sqrt{1-\tau}b, \quad (2.23)$$

and the probability of counts reads

$$\begin{aligned} p_\tau(m) &= \text{Tr} [U_\tau \rho \otimes |0\rangle\langle 0| U_\tau^\dagger |m\rangle\langle m| \otimes 1] \\ &= \sum_{n=m}^{\infty} \rho_{nn} \binom{n}{m} (1-\tau)^{n-m} \tau^m. \end{aligned} \quad (2.24)$$

Equation (2.24) reproduces the probability distribution of (2.21) with  $\tau = \eta$ . We conclude that a photo-detector of quantum efficiency  $\eta$  is equivalent to a perfect photo-detector preceded by a beam splitter of transmissivity  $\eta$  which accounts for the overall losses of the detection process.

### 2.3.2 Balanced Homodyne Detection

The balanced homodyne detector provides the measurement of the quadrature of the field  $X_\varphi$  in (2.8). It was proposed by Yuen and Chan [40], and subsequently demonstrated by Abbas, Chan and Yee [41].

The scheme of a balanced homodyne detector is depicted in Fig. 2.1. The signal mode  $a$  interferes with a strong laser beam mode  $b$  in a balanced 50/50 beam splitter. The mode  $b$  is so-called *local oscillator* (LO) mode of the detector. It operates at the same frequency of  $a$ , and is excited by the laser in a strong coherent state  $|z\rangle$ . Since in all experiments that use homodyne detectors the signal and the LO beams are generated by a common source, we assume that they have a fixed phase relation. In this case the LO phase provides a reference for the quadrature measurement, namely we identify the phase of the LO with the phase difference between the two modes. As we will see, by tuning  $\varphi = \arg z$  we can measure the quadrature  $X_\varphi$  at different phases.

After the beam splitter the two modes are detected by two identical photodetectors (usually linear avalanche photodiodes), and finally the difference of photocurrents at zero frequency is electronically processed and rescaled by

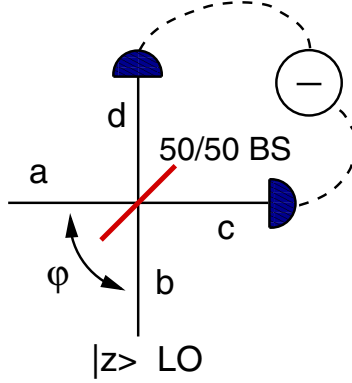


**Fig. 2.1.** Scheme of the balanced homodyne detector.

$2|z|$ . According to (2.22), the modes at the output of the 50/50 beam splitter ( $\tau = 1/2$ ) write

$$c = \frac{a-b}{\sqrt{2}}, \quad d = \frac{a+b}{\sqrt{2}}, \quad (2.25)$$

hence the difference of photocurrents is given by the following operator

$$I = \frac{d^\dagger d - c^\dagger c}{2|z|} = \frac{a^\dagger b + b^\dagger a}{2|z|}. \quad (2.26)$$

Let us now proceed to evaluate the probability distribution of the output photocurrent  $I$  for a generic state  $\rho$  of the signal mode  $a$ . In the following treatment we will follow [42, 43].

Let us consider the moments generating function of the photocurrent  $I$

$$\chi(\lambda) = \text{Tr} [\rho \otimes |z\rangle\langle z| e^{i\lambda I}], \quad (2.27)$$

which provides the probability distribution of  $I$  as the Fourier transform

$$P(I) = \int_{-\infty}^{+\infty} \frac{d\lambda}{2\pi} e^{-i\lambda I} \chi(\lambda). \quad (2.28)$$

Using the BCH formula [44, 45] for the  $SU(2)$  group, namely

$$\exp(\xi a b^\dagger - \xi^* a^\dagger b) = e^{\zeta b^\dagger a} (1 + |\zeta|^2)^{\frac{1}{2}(b^\dagger b - a^\dagger a)} e^{-\zeta^* a^\dagger b}, \quad \zeta = \frac{\xi}{|\xi|} \tan |\xi|, \quad (2.29)$$

one can write the exponential in (2.27) in normal-ordered form with respect to mode  $b$  as follows

$$\chi(\lambda) = \left\langle e^{i \tan\left(\frac{\lambda}{2|z|}\right) b^\dagger a} \left[ \cos\left(\frac{\lambda}{2|z|}\right) \right]^{a^\dagger a - b^\dagger b} e^{i \tan\left(\frac{\lambda}{2|z|}\right) a^\dagger b} \right\rangle_{ab}. \quad (2.30)$$

Since mode  $b$  is in a coherent state  $|z\rangle$  the partial trace over  $b$  can be evaluated as follows

$$\begin{aligned} \chi(\lambda) &= \left\langle e^{i \tan\left(\frac{\lambda}{2|z|}\right) z^* a} \left[ \cos\left(\frac{\lambda}{2|z|}\right) \right]^{a^\dagger a} e^{i \tan\left(\frac{\lambda}{2|z|}\right) z a^\dagger} \right\rangle_a \\ &\times \left\langle z \left| \left[ \cos\left(\frac{\lambda}{2|z|}\right) \right]^{-b^\dagger b} \right| z \right\rangle. \end{aligned} \quad (2.31)$$

Using now (2.13), one can rewrite (2.31) in normal order with respect to  $a$ , namely

$$\chi(\lambda) = \left\langle e^{i z \sin\left(\frac{\lambda}{2|z|}\right) a^\dagger} \exp\left[-2 \sin^2\left(\frac{\lambda}{4|z|}\right) (a^\dagger a + |z|^2)\right] e^{i z^* \sin\left(\frac{\lambda}{2|z|}\right) a} \right\rangle_a, \quad (2.32)$$

In the strong-LO limit  $z \rightarrow \infty$ , only the lowest order terms in  $\lambda/|z|$  are retained,  $a^\dagger a$  is neglected with respect to  $|z|^2$ , and (2.32) simplifies as follows

$$\lim_{z \rightarrow \infty} \chi(\lambda) = \left\langle e^{i \frac{\lambda}{2} e^{i\varphi} a^\dagger} \exp\left[-\frac{\lambda^2}{8}\right] e^{i \frac{\lambda}{2} e^{-i\varphi} a} \right\rangle_a = \langle \exp[i\lambda X_\varphi] \rangle_a, \quad (2.33)$$

where  $\varphi = \arg z$ . The generating function in (2.33) is then equivalent to the POVM

$$\Pi(x) = \int_{-\infty}^{+\infty} \frac{d\lambda}{2\pi} \exp[i\lambda(X_\varphi - x)] = \delta(X_\varphi - x) \equiv |x\rangle_\varphi \langle x|, \quad (2.34)$$

namely the projector on the eigenstate of the quadrature  $X_\varphi$  with eigenvalue  $x$ . In conclusion, the balanced homodyne detector achieves the ideal measurement of the quadrature  $X_\varphi$  in the strong LO limit. In this limit, the probability distribution of the output photocurrent  $I$  approaches exactly the probability distribution  $p(x, \varphi) = {}_\varphi \langle x | \rho | x \rangle_\varphi$  of the quadrature  $X_\varphi$ , and this for any state  $\rho$  of the signal mode  $a$ .

It is easy to take into account non-unit quantum efficiency at detectors. According to (2.23) one has the replacements

$$c \implies \sqrt{\eta}c - \sqrt{1-\eta}u, \quad u, v \text{ vacuum modes} \quad (2.35)$$

$$d \implies \sqrt{\eta}d - \sqrt{1-\eta}v, \quad (2.36)$$

and now the output current is rescaled by  $2|z|\eta$ , namely

$$I_\eta \simeq \frac{1}{2|z|} \left\{ \left[ a + \sqrt{\frac{1-\eta}{2\eta}}(u+v) \right] b^\dagger + h.c \right\}, \quad (2.37)$$

where only terms containing the strong LO mode  $b$  are retained. The POVM is then obtained by replacing

$$X_\varphi \rightarrow X_\varphi + \sqrt{\frac{1-\eta}{2\eta}}(u_\varphi + v_\varphi) \quad (2.38)$$

in (2.34), with  $w_\varphi = (w^\dagger e^{i\varphi} + w e^{-i\varphi})/2$ ,  $w = u, v$ , and tracing the vacuum modes  $u$  and  $v$ . One then obtains

$$\begin{aligned} \Pi_\eta(x) &= \int_{-\infty}^{+\infty} \frac{d\lambda}{2\pi} e^{i\lambda(X_\varphi - x)} |\langle 0 | e^{i\lambda\sqrt{\frac{1-\eta}{2\eta}}u_\varphi} | 0 \rangle|^2 = \int_{-\infty}^{+\infty} \frac{d\lambda}{2\pi} e^{i\lambda(X_\varphi - x)} e^{-\lambda^2 \frac{1-\eta}{8\eta}} \\ &= \frac{1}{\sqrt{2\pi\Delta_\eta^2}} \int_{-\infty}^{+\infty} dx' e^{-\frac{1}{2\Delta_\eta^2}(x-x')^2} |x'\rangle_{\varphi\varphi} \langle x'|, \end{aligned} \quad (2.39)$$

where  $\Delta_\eta^2 = \frac{1-\eta}{4\eta}$ . Thus the POVM, and in turn the probability distribution of the output photocurrent, are just the Gaussian convolution of the ideal ones with rms  $\Delta_\eta$ .

### 2.3.3 Heterodyne Detection

Heterodyne detection allows one to perform the joint measurement of two conjugated quadratures of the field [46, 47]. The scheme of the heterodyne detector is depicted in Fig. 2.2.

A strong local oscillator at frequency  $\omega$  in a coherent state  $|\alpha\rangle$  hits a beam splitter with transmissivity  $\tau \rightarrow 1$ , and with the coherent amplitude  $\alpha$  such that  $\gamma \equiv |\alpha|\sqrt{\tau(1-\tau)}$  is kept constant. If the output photocurrent is sampled at the intermediate frequency  $\omega_{IF}$ , just the field modes  $a$  and  $b$  at frequency  $\omega \pm \omega_{IF}$  are selected by the detector. Modes  $a$  and  $b$  are usually referred to as signal band and image band modes, respectively. In the strong LO limit, upon tracing the LO mode, the output photocurrent  $I(\omega_{IF})$  rescaled by  $\gamma$  is equivalent to the complex operator

$$Z = \frac{I(\omega_{IF})}{\gamma} = a - b^\dagger, \quad (2.40)$$

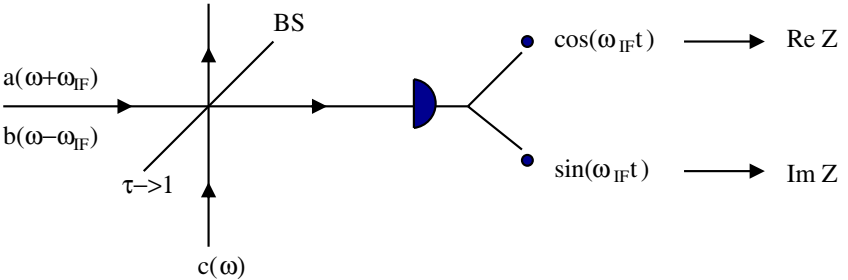


Fig. 2.2. Scheme of the heterodyne detector.

where the arbitrary phases of modes have been suitably chosen. The heterodyne photocurrent  $Z$  is a normal operator, equivalent to a couple of commuting selfadjoint operators

$$Z = \text{Re}Z + i\text{Im}Z, \quad [Z, Z^\dagger] = [\text{Re}Z, \text{Im}Z] = 0. \quad (2.41)$$

The POVM of the detector is then given by the orthogonal eigenvectors of  $Z$ . It is convenient to introduce the notation of [48] for vectors in the tensor product of Hilbert spaces  $\mathcal{H} \otimes \mathcal{H}$

$$|A\rangle\rangle = \sum_{nm} A_{nm} |n\rangle \otimes |m\rangle \equiv (A \otimes I)|I\rangle\rangle \equiv (I \otimes A^\tau)|I\rangle\rangle, \quad (2.42)$$

where  $A^\tau$  denotes the transposed operator with respect to some pre-chosen orthonormal basis. Equation (2.42) exploits the isomorphism between the Hilbert space of the Hilbert-Schmidt operators  $A, B \in \text{HS}(\mathcal{H})$  with scalar product  $\langle A, B \rangle = \text{Tr}[A^\dagger B]$ , and the Hilbert space of bipartite vectors  $|A\rangle\rangle, |B\rangle\rangle \in \mathcal{H} \otimes \mathcal{H}$ , where one has  $\langle\langle A|B\rangle\rangle \equiv \langle A, B \rangle$ .

Using the above notation it is easy to write the eigenvectors of  $Z$  with eigenvalue  $z$  as  $\frac{1}{\sqrt{\pi}}|D(z)\rangle\rangle$ . In fact one has [49]

$$\begin{aligned} Z|D(z)\rangle\rangle &= (a - b^\dagger)(D_a(z) \otimes I_b)|I\rangle\rangle = (D_a(z) \otimes I_b)(a - b^\dagger + z) \sum_{n=0}^{\infty} |n\rangle \otimes |n\rangle \\ &= z(D_a(z) \otimes I_b)|I\rangle\rangle = z|D(z)\rangle\rangle. \end{aligned} \quad (2.43)$$

The orthogonality of such eigenvectors can be verified through the relation

$$\langle\langle D(z)|D(z')\rangle\rangle = \text{Tr}[D^\dagger(z)D(z')] = \pi\delta^{(2)}(z - z'), \quad (2.44)$$

where  $\delta^{(2)}(\alpha)$  denotes the Dirac delta function over the complex plane

$$\delta^{(2)}(\alpha) = \int_{\mathbb{C}} \frac{d^2\gamma}{\pi^2} \exp(\gamma\alpha^* - \gamma^*\alpha). \quad (2.45)$$

In conventional heterodyne detection the image band mode is in the vacuum state, and one is just interested in measuring the field mode  $a$ . In this case we can evaluate the POVM upon tracing on mode  $b$ . One has

$$\begin{aligned} \Pi(z, z^*) &= \frac{1}{\pi} \text{Tr}_b[|D(z)\rangle\rangle\langle\langle D(z)|I_a \otimes |0\rangle\langle 0|] \\ &= \frac{1}{\pi} D(z)|0\rangle\langle 0|D^\dagger(z) = \frac{1}{\pi} |z\rangle\langle z|. \end{aligned} \quad (2.46)$$

Namely, one obtains the projectors on coherent states. The coherent-state POVM provides the optimal joint measurement of conjugated quadratures of the field [50]. In fact, heterodyne detection allows one to measure the Q-function in (2.4). According to (2.3) then it provides the expectation value

of anti-normal ordered field operator. For a state  $\rho$  the expectation value of any quadrature  $X_\varphi$  is obtained as

$$\langle X_\varphi \rangle = \text{Tr}[\rho X_\varphi] = \int_{\mathbb{C}} \frac{d^2\alpha}{\pi} \text{Re}(\alpha e^{-i\varphi}) Q(\alpha, \alpha^*). \quad (2.47)$$

The price to pay for jointly measuring a pair of non commuting observables is an additional noise. The rms fluctuation is evaluated as follows

$$\int_{\mathbb{C}} \frac{d^2\alpha}{\pi} [\text{Re}(\alpha e^{-i\varphi})]^2 Q(\alpha, \alpha^*) - \langle X_\varphi \rangle^2 = \langle \Delta X_\varphi^2 \rangle + \frac{1}{4}, \quad (2.48)$$

where  $\langle \Delta X_\varphi^2 \rangle$  is the intrinsic noise, and the additional term is usually referred to as “the additional 3dB noise due to the joint measure” [51–53].

The effect of non-unit quantum efficiency can be taken into account in analogous way as in Sect. 2.3.2 for homodyne detection. The heterodyne photocurrent is rescaled by an additional factor  $\eta^{1/2}$ , and vacuum modes  $u$  and  $v$  are introduced, thus giving [54]

$$Z_\eta = a - b^\dagger + \sqrt{\frac{1-\eta}{\eta}} u - \sqrt{\frac{1-\eta}{\eta}} v^\dagger. \quad (2.49)$$

Upon tracing over modes  $u$  and  $v$ , one obtain the POVM

$$\begin{aligned} \Pi_\eta(z, z^*) &= \int_{\mathbb{C}} \frac{d^2\gamma}{\pi^2} {}_u\langle 0|_v \langle 0| e^{\gamma(Z_\eta^\dagger - z^*) - \gamma^*(Z_\eta - z)} |0\rangle_u |0\rangle_v \\ &= \int_{\mathbb{C}} \frac{d^2\gamma}{\pi^2} e^{\gamma(Z^\dagger - z^*) - \gamma^*(Z - z)} e^{-\frac{1-\eta}{\eta} |\gamma|^2} \\ &= \frac{\eta}{\pi(1-\eta)} e^{-\frac{\eta}{1-\eta} |Z - z|^2} = \int_{\mathbb{C}} \frac{d^2z'}{\pi \Delta_\eta^2} e^{-\frac{|z' - z|^2}{\Delta_\eta^2}} |D(z')\rangle \langle\langle D(z')|. \end{aligned} \quad (2.50)$$

The probability distribution is then a Gaussian convolution on the complex plane of the ideal probability with rms  $\Delta_\eta^2 = (1-\eta)/\eta$ .

Analogously, the coherent-state POVM for conventional heterodyne detection with vacuum image band mode is replaced with

$$\Pi_\eta(z, z^*) = \int_{\mathbb{C}} \frac{d^2z'}{\pi \Delta_\eta^2} e^{-\frac{|z' - z|^2}{\Delta_\eta^2}} |z'\rangle \langle z'|. \quad (2.51)$$

From (2.9) we can equivalently say that the heterodyne detection probability density is given by the generalized Wigner function  $W_s(\alpha, \alpha^*)$ , with  $s = 1 - \frac{2}{\eta}$ . Notice that for  $\eta < 1$ , the average of functions  $\alpha^n \alpha^{*m}$  is related to the expectation value of a different ordering of field operators. However, one has the relevant identity [29, 55]

$$:(a^\dagger)^n a^m :_s = \sum_{k=0}^{\min(n,m)} k! \binom{n}{k} \binom{m}{k} \left(\frac{t-s}{2}\right)^k :(a^\dagger)^{n-k} a^{m-k} :_t, \quad (2.52)$$

where  $(n, m) = \min(n, m)$ , and then

$$\begin{aligned} & \int_{\mathbb{C}} d^2\alpha W_{1-\frac{2}{\eta}}(\alpha, \alpha^*) \alpha^m \alpha^{*n} \\ &= \sum_{k=0}^{(n,m)} k! \binom{n}{k} \binom{m}{k} \left(\frac{1-\eta}{\eta}\right)^k \langle a^{m-k} (a^\dagger)^{n-k} \rangle. \end{aligned} \quad (2.53)$$

Notice that the measure of the Q-function (or any smoothed version for  $\eta < 1$ ) does not allow one to recover the expectation value of *any* operator through an average over heterodyne outcomes. In fact, one needs the admissibility of anti-normal ordered expansion [56] and the convergence of the integral in (2.53). In particular, the matrix elements of the density operator cannot be recovered.

Finally, it is worth mentioning that the above results hold also for an image-band mode with the same frequency of the signal. In this case a measurement scheme based on multipoint homodyne detection should be used [47, 55, 57–63].

## 2.4 General Tomographic Method

In the first part of the section a brief history of tomography is presented. Then, we give a sketch of the conventional medical tomography, and we show its analogy with the optical homodyne tomography for the reconstruction of the Wigner function proposed by Vogel and Risken [7]. However the limits and the intrinsic unreliability of this method are explained.

The first exact method was given in [8], and successively refined in [9]. It allows the reconstruction of the density matrix  $\rho$ , bypassing the inversion of the Wigner function. Analogously, it provides the expectation values of arbitrary operators, directly as an average of “Kernel functions” evaluated on the experimental data collected by homodyne detection.

The general tomographic method is presented in Sect. 2.4.4. The concept of “quorum”, namely the complete set of observables whose measurement provides the expectation value of any desired operator, is introduced. We show that some “orthogonality” and “completeness” relations in the linear algebra of operators are sufficient to individuate a quorum [26].

In Sect. 2.4.9 some developments of the basic tomographic method are shown. First, the deconvolution of noise given by the imperfections of detectors and/or experimental apparatus. Such noise can be eliminated under the hypothesis that the pertaining CP-map is invertible [20]. Then, we show that also the statistical random noise can be reduced through the adaptive tomography technique [22].

The relevant topic of multimode tomography with a single oscillator is given separate treatment in the following section.

### 2.4.1 Brief Historical Excursus

The problem of quantum state determination through repeated measurements on identically prepared systems was already stated in 1957 by Fano [5]. He was aware that more than two observables are needed for this purpose. It was only with the proposal by Vogel and Risken [7] however, that quantum tomography was born. The first experiments, which already showed reconstructions of coherent and squeezed states were performed in Michael Raymer's group at the University of Oregon [6]. The main idea at the basis of the first proposal is that it is possible to extend to the quantum domain the algorithms that are conventionally used in medical imaging to recover two dimensional distributions (say of mass) from unidimensional projections in different directions. However, the first tomographic method is unreliable for the measurement of unknown quantum states, since some arbitrary smoothing parameters have to be introduced. The exact unbiased tomographic procedure was proposed in [8], and successively simplified in [9]. The exact homodyne method has been implemented experimentally to measure the photon statistics of a semiconductor laser [10], and the density matrix of a squeezed vacuum [11]. The success of optical homodyne tomography has then stimulated the development of state-reconstruction procedures for atomic beams [12], the experimental determination of the vibrational state of a molecule [13], of an ensemble of helium atoms [14], and of a single ion in a Paul trap [15].

More recently, quantum tomography has been generalized to the estimation of an arbitrary observable of the field [16], with any number of modes [17], and, finally, to arbitrary quantum systems via group theory [18, 20, 21]. Further developments such as noise deconvolution [20] and adaptive tomography [22] were found. The use of max-likelihood strategies [23] has made possible to reduce dramatically the number of experimental data (by a factor  $10^3 \div 10^5$ !) with negligible bias for most practical cases of interest. Finally, very recently, a method for tomographic estimation of the unknown quantum operation of a quantum device has been presented [27], where a fixed input entangled state is used. Similarly, one can also estimate the ensemble average of all operators by measuring only one fixed "universal" observable on an extended Hilbert space [64]. The latest development [26] deduces the general tomographic method from the property of spanning sets of operators. In fact, the group structure is not necessary to individuate a "quorum", but just some "orthogonality" and "completeness" relations in the linear algebra of operators are sufficient to that purpose. The general method will be presented in this context.

### 2.4.2 Conventional Tomographic Imaging

In conventional medical tomography, one collects data in the form of marginal distributions of the mass function  $m(x, y)$ . In the complex plane the marginal

$r(x, \varphi)$  is a projection of the complex function  $m(x, y)$  on the direction indicated by the angle  $\varphi \in [0, \pi]$ , namely

$$r(x, \varphi) = \int_{-\infty}^{+\infty} \frac{dy}{\pi} m((x + iy)e^{i\varphi}, (x - iy)e^{-i\varphi}). \quad (2.54)$$

The collection of marginals for different  $\varphi$  is called “Radon transform”. The tomography process essentially consists in the inversion of the Radon transform (2.54), in order to recover the mass function  $m(x, y)$  from the marginals  $r(x, \varphi)$ .

Here we derive inversion of (2.54). Consider the identity

$$m(\alpha, \alpha^*) = \int_{\mathbb{C}} d^2\beta \delta^{(2)}(\alpha - \beta) m(\beta, \beta^*), \quad (2.55)$$

where  $\delta^{(2)}(\alpha)$  denotes the Dirac delta function of (2.45), and  $m(\alpha, \alpha^*) \equiv m(x, y)$ , with  $\alpha = x + iy$  and  $\alpha^* = x - iy$ . Equation (2.45) rewrites

$$\delta^{(2)}(\alpha) = \int_0^{+\infty} \frac{dk}{4} k \int_0^{2\pi} \frac{d\varphi}{\pi^2} e^{-ik\alpha\varphi} = \int_{-\infty}^{+\infty} \frac{dk}{4} |k| \int_0^\pi \frac{d\varphi}{\pi^2} e^{-ik\alpha\varphi}, \quad (2.56)$$

with  $\alpha_\varphi \equiv \text{Re}(\alpha e^{-i\varphi}) = -\alpha_{\varphi+\pi}$ . From (2.55) and (2.56) the inverse Radon transform is obtained as follows

$$m(x, y) = \int_0^\pi \frac{d\varphi}{\pi} \int_{-\infty}^{+\infty} dx' r(x', \varphi) \int_{-\infty}^{+\infty} \frac{dk}{4} |k| e^{ik(x' - \alpha_\varphi)}. \quad (2.57)$$

Equation (2.57) is conventionally written as

$$m(x, y) = \int_0^\pi \frac{d\varphi}{\pi} \int_{-\infty}^{+\infty} dx' r(x', \varphi) K(x' - \alpha_\varphi), \quad (2.58)$$

where  $K(x)$  is given by

$$K(x) \equiv \int_{-\infty}^{+\infty} \frac{dk}{4} |k| e^{ikx} = \frac{1}{2} \text{Re} \int_0^{+\infty} dk k e^{ikx} = -\frac{1}{2} \mathcal{P} \frac{1}{x^2}, \quad (2.59)$$

with  $\mathcal{P}$  denoting the Cauchy principal value. Integrating by parts (2.58) one obtains the tomographic formula that is usually found in medical imaging, *i.e.*

$$m(x, y) = \frac{1}{2\pi} \int_0^\pi d\varphi \mathcal{P} \int_{-\infty}^{+\infty} dx' \frac{1}{x' - \alpha_\varphi} \frac{\partial}{\partial x'} r(x', \varphi), \quad (2.60)$$

which allows the reconstruction of the mass distribution  $m(x, y)$  from its projections along different directions  $r(x, \varphi)$ .

### 2.4.3 Extension to the Quantum Domain

In the quantum imaging process one would like to reconstruct a quantum state in the form of its Wigner function, by starting from its marginal probability distributions. As shown in Sect. 2.2, the Wigner function is a real normalized function that is in one-to-one correspondence with the state density operator  $\rho$ . As noticed in (2.7), the probability distributions of the quadrature operators  $X_\varphi = (a^\dagger e^{i\varphi} + a e^{-i\varphi})/2$  are the marginal probabilities of the Wigner function for the state  $\rho$ . Thus, by applying the same procedure outlined in the previous subsection, Vogel and Risken [7] proposed a method to recover the Wigner function *via* an inverse Radon transform from the quadrature probability distributions  $p(x, \varphi)$ , namely

$$W(x, y) = \int_0^\pi \frac{d\varphi}{\pi} \int_{-\infty}^{+\infty} dx' p(x', \varphi) \int_{-\infty}^{+\infty} \frac{dk}{4} |k| e^{ik(x' - x \cos \varphi - y \sin \varphi)}. \quad (2.61)$$

Notice that in the original paper [7] conventional tomographic imaging is never referred to. As shown in Sect. 2.3.2 the experimental data, distributed according to the quadrature probability density, can be obtained by using the homodyne detector which measures the quadrature of the field. The method proposed by Vogel and Risken, namely the inversion of the Radon transform, was the one which has been used in the first experiments [6].

However, this first method is unreliable for the reconstruction of unknown quantum states, since there is an intrinsic unavoidable systematic error. In fact the integral on  $k$  in (2.61) is unbounded. In order to use the inverse Radon transform, one would need the analytical form of the marginal distribution of the quadrature  $p(x, \varphi)$ . This can be obtained by collecting the experimental data into histograms and splining these histograms. This is not an unbiased procedure since the degree of splining, the width of the histogram bins and the number of different phases on which the experimental data should be collected are arbitrary parameters and introduce systematic errors whose effects cannot be easily controlled. For example, the effect of using high degrees of splining is the wash-out of the quantum features of the state, and, *vice-versa*, the effect of low degrees of splining is to create negative bias for the probabilities in the reconstruction (see [8] for details).

A new approach to optical tomography was proposed in [8]. This approach, that will be referred to as ‘quantum homodyne tomography’, allows one to recover the quantum state of the field  $\rho$  (and also the mean values of arbitrary operators) directly from the data, abolishing all the sources of systematic errors. Only statistical errors are present, and they can be reduced arbitrarily by collecting more experimental data. The correct method will be derived from the general tomographic theory in Sect. 2.4.5.

### 2.4.4 General Method of Quantum Tomography

In the following the general method of quantum tomography will be explained. First, we give the basics of Monte Carlo integral theory which are

needed to implement the tomographic algorithms in actual experiments and in numerical simulations. Then, we derive the formulas on which all schemes of state reconstruction are based.

## Basic Statistics

The aim of quantum tomography is to estimate, in arbitrary quantum systems, the mean value  $\langle O \rangle$  of a system operator  $O$  using only the results of the measurements on a set of observables  $\{Q_\lambda, \lambda \in \Lambda\}$ , called “quorum”. The procedure by which this can be obtained needs the so called “Kernel function”  $\mathcal{R}_\lambda[O](x_\lambda)$  which is a function of the eigenvalues  $x_\lambda$  of the quorum operators. Integrating the Kernel with the probability  $p_\lambda(x_\lambda)$  of having outcome  $x_\lambda$  when measuring  $Q_\lambda$ , the mean value of  $O$  is obtained as follows

$$\langle O \rangle = \int_\Lambda d\lambda \int_{-\infty}^{+\infty} dx_\lambda p_\lambda(x_\lambda) \mathcal{R}_\lambda[O](x_\lambda), \quad (2.62)$$

where the first integral is performed on the values of  $\lambda$  that designate all quorum observables, and the second on the eigenvalues of the quorum observable  $Q_\lambda$  determined by the  $\lambda$  variable of the outer integral. Both integrals in (2.62) can suitably be replaced by sums.

The algorithm to estimate  $\langle O \rangle$  with (2.62) is the following. One chooses a quorum operator  $Q_\lambda$  by choosing  $\lambda$  with uniform probability in  $\Lambda$  and performs a measurement, obtaining the result  $x_i$ . By repeating the procedure  $N$  times, one collects the set of experimental data  $\{(\lambda_i, x_i), \text{ with } i = 1, \dots, N\}$ , where  $\lambda_i$  identifies the quorum observable used for the  $i$ th measurement, and  $x_i$  its result. From the same set of data the mean value of any operator  $O$  can be obtained. In fact, one evaluates the Kernel function for  $O$  and the quorum  $Q_\lambda$ , and then samples the double integral of (2.62) using the limit

$$\langle O \rangle = \lim_{N \rightarrow \infty} \frac{1}{N} \sum_{i=1}^N \mathcal{R}_{\lambda_i}[O](x_i). \quad (2.63)$$

Of course the finite sum,

$$F_N = \frac{1}{N} \sum_{i=1}^N \mathcal{R}_{\lambda_i}[O](x_i), \quad (2.64)$$

gives an approximation of  $\langle O \rangle$ . To estimate the error in the approximation one applies the central limit theorem that we recall here.

**Central limit theorem.** Consider  $N$  statistically uncorrelated random variables  $\{z_i, i = 1, \dots, N\}$ , with mean values  $\mu(z_i)$ , variances  $\sigma^2(z_i)$  and bounded third order moments. If the variances  $\sigma^2(z_i)$  are all of the same

order then the statistical variable “sum”  $y$  defined as

$$y = \sum_{i=1}^N z_i \quad (2.65)$$

has mean and variance

$$\mu(y) = \sum_{i=1}^N \mu(z_i), \quad \sigma^2(y) = \sum_{i=1}^N \sigma^2(z_i). \quad (2.66)$$

The distribution of  $y$  approaches asymptotically a Gaussian for  $N \rightarrow \infty$ . In practical cases, the distribution of  $y$  can be considered Gaussian already for  $N$  as low as  $N \sim 10$ .

For our needs the hypotheses are met if the Kernel function  $\mathcal{R}_{\lambda_i}[O](x_i)$  in (2.64) has limited moments up to the third order, since  $x_i$  come from the same probability density, and hence all  $z_i = \frac{1}{N}\mathcal{R}_{\lambda_i}[O](x_i)$  have the same mean  $\mu(z_i) = \frac{1}{N}\langle O \rangle$  and variance

$$\sigma^2(z_i) = \frac{1}{N^2} \left[ \lim_{M \rightarrow \infty} \sum_{j=1}^M \mathcal{R}_{\lambda_i}^2[O](x_j) - \langle O \rangle^2 \right]. \quad (2.67)$$

Using the central limit theorem, we can conclude that the experimental average  $y \equiv F_N$  in (2.64) is a statistical variable distributed as a Gaussian with mean value  $\mu(y) = \langle O \rangle$  and variance

$$\sigma^2(y) = \frac{1}{N} \left[ \lim_{M \rightarrow \infty} \frac{1}{M} \sum_{j=1}^M \mathcal{R}_{\lambda_i}^2[O](x_j) - \langle O \rangle^2 \right]. \quad (2.68)$$

Then the tomographic estimation converges with statistical error that decreases as  $N^{-1/2}$ .

Since the statistical variable  $F_N$  converges to  $\langle O \rangle$  and is distributed as a Gaussian we can also evaluate the statistical error that affects the tomographic reconstruction. Upon dividing the experimental data into  $M$  statistical blocks of equal dimension one evaluates the average in (2.64) for each block. A set  $F_n$  ( $n = 1, 2, \dots, M$ ) is then obtained and it is Gaussian distributed with mean value

$$m = \frac{1}{M} \sum_{n=1}^M F_n \quad (2.69)$$

and variance

$$s^2 = \frac{1}{M-1} \sum_{n=1}^M (F_n - m)^2. \quad (2.70)$$

Notice that the factor  $1/(M-1)$  in the variance comes from the fact that we are using the “experimental” estimated mean value  $m$  in place of the “real” one  $\mu$ . The variance of the mean  $m$  is given by

$$\sigma^2(m) \equiv \sigma^2 \left( \frac{1}{M} \sum_{n=1}^M F_n \right) = \frac{1}{M^2} \sum_{n=1}^M \sigma^2(F_n) = \frac{1}{M} s^2, \quad (2.71)$$

and thus the error on the mean  $m$  estimated from the data is given by

$$\epsilon = \frac{s}{\sqrt{M}} = \sqrt{\sum_{n=1}^M \frac{(F_n - m)^2}{M(M-1)}}. \quad (2.72)$$

The usual statistical interpretation applies: the “real” value  $\mu = \langle O \rangle$  is to be found in the interval  $[m - \epsilon, m + \epsilon]$  with  $\sim 68\%$  probability, in  $[m - 2\epsilon, m + 2\epsilon]$  with  $\sim 95\%$  probability, and in  $[m - 3\epsilon, m + 3\epsilon]$  with  $\sim$  unit probability. In order to test that the confidence intervals are estimated correctly, one can check that the  $F_n$  distribution is actually Gaussian. This can be done by comparing the histogram of the block data with a Gaussian, or by using the  $\chi^2$  test.

## Characterization of the Quorum

As we will see, different estimation techniques have been proposed tailored to different systems, such as the radiation field [9, 17], trapped ions and molecular vibrational states [65], spin systems [66], etc. As a matter of fact, all these schemes can be embodied in the following approach.

The tomographic reconstruction of an operator  $O$  is possible when there exists a resolution of the form

$$O = \int_{\Lambda} d\lambda \operatorname{Tr} [OB^\dagger(\lambda)] C(\lambda), \quad (2.73)$$

where  $\lambda$  is a (possibly multidimensional) parameter living on a (discrete or continuous) manifold  $\Lambda$ . The only hypothesis in (2.73) is the existence of the trace. If, for example,  $O$  is a trace-class operator, then we do not need to require  $B(\lambda)$  to be of Hilbert-Schmidt class, since it is sufficient to require  $B(\lambda)$  bounded. The operators  $C(\lambda)$  are functions of the quorum of observables measured for the reconstruction, whereas the operators  $B(\lambda)$  form the *dual basis* of the set  $C(\lambda)$ . The term

$$\mathcal{E}[O](\lambda) = \operatorname{Tr} [OB^\dagger(\lambda)] C(\lambda) \quad (2.74)$$

represents the quantum estimator for the operator  $O$ . The expectation value of  $O$  is given by the ensemble average

$$\langle O \rangle \equiv \operatorname{Tr} [O\rho] = \int_{\Lambda} d\lambda \operatorname{Tr} [OB^\dagger(\lambda)] \operatorname{Tr} [C(\lambda)\rho] \equiv \int_{\Lambda} d\lambda \langle \mathcal{E}[O](\lambda) \rangle, \quad (2.75)$$

where  $\rho$  is the density matrix of the quantum system under investigation. Notice that the quantity  $\text{Tr}[C(\lambda)\rho]$  depends only on the quantum state, and it is related to the probability distribution of the measurement outcomes, whereas the term  $\text{Tr}[OB^\dagger(\lambda)]$  depends only on the quantity to be measured. In particular, the tomography of the quantum state of a system corresponds to writing (2.73) for the operators  $O = |k\rangle\langle n|$ ,  $\{|n\rangle\}$  being a given Hilbert space basis. For a given system, the existence of a set of operators  $C(\lambda)$ , together with its dual basis  $B(\lambda)$  allows universal quantum estimation, i. e. the reconstruction of any operator.

We now give two characterizations of the sets  $B(\lambda)$  and  $C(\lambda)$  that are necessary and sufficient conditions for writing (2.73).

### Condition 1: Bi-orthogonality

Let us consider a complete orthonormal basis of vectors  $|n\rangle$  ( $n = 0, 1, \dots$ ). Formula (2.73) is equivalent to the bi-orthogonality condition

$$\int_A d\lambda \langle q|B^\dagger(\lambda)|p\rangle \langle m|C(\lambda)|l\rangle = \delta_{mp}\delta_{lq}, \quad (2.76)$$

where  $\delta_{ij}$  is the Kronecker delta. Equation (2.76) can be straightforwardly generalized to a continuous basis.

### Condition 2: Completeness

If the set of operators  $C(\lambda)$  is *irreducible*, namely if any operator can be written as a linear combination of the  $C(\lambda)$  as

$$O = \int_A d\lambda a(\lambda) C(\lambda), \quad (2.77)$$

then (2.73) is also equivalent to the trace condition

$$\text{Tr}[B^\dagger(\lambda)C(\mu)] = \delta(\lambda, \mu), \quad (2.78)$$

where  $\delta(\lambda, \mu)$  is a *reproducing kernel* for the set  $B(\lambda)$ , namely a function or a tempered distribution which satisfies

$$\int_A d\lambda B(\lambda) \delta(\lambda, \mu) = B(\mu). \quad (2.79)$$

An analogous identity holds for the set of  $C(\lambda)$

$$\int_A d\lambda C(\lambda) \delta(\lambda, \mu) = C(\mu). \quad (2.80)$$

The proofs are straightforward. The irreducibility condition on the operators  $C(\lambda)$  is essential for the equivalence of (2.73) and (2.78). A simple counterexample is provided by the set of projectors  $P(x) = |x\rangle\langle x|$  over the eigenstates

of a selfadjoint operator  $X$ . In fact, (2.78) is satisfied by  $P(x)$ . However, since they do not form an irreducible set, it is not possible to express a generic operator as  $O \neq \int_{\mathcal{X}} dx \langle x|O|x \rangle |x\rangle\langle x|$ .

If either the set  $B(\lambda)$  or the set  $C(\lambda)$  satisfy the additional trace condition

$$\text{Tr} [B^\dagger(\mu)B(\lambda)] = \delta(\lambda, \mu) , \quad (2.81)$$

$$\text{Tr} [C^\dagger(\mu)C(\lambda)] = \delta(\lambda, \mu) , \quad (2.82)$$

then we have  $C(\lambda) = B(\lambda)$  (notice that neither  $B(\lambda)$  nor  $C(\lambda)$  need to be unitary). In this case, (2.73) can be rewritten as

$$O = \int_A d\lambda \text{Tr} [OC^\dagger(\lambda)] C(\lambda) . \quad (2.83)$$

A set of observables  $Q_\lambda$  constitute a quorum when there are functions  $f_\lambda(Q_\lambda) = C(\lambda)$  so that  $C(\lambda)$  form an irreducible set. The quantum estimator for  $O$  in (2.74) then writes as a function of the quorum operators

$$\mathcal{E}[O](\lambda) \equiv \mathcal{E}_\lambda[O](Q_\lambda) . \quad (2.84)$$

Notice that if a set of observables  $Q_\lambda$  constitutes a quorum, than the set of projectors  $|q\rangle_{\lambda\lambda}\langle q|$  over their eigenvectors provides a quorum too, with the measure  $d\lambda$  in (2.73) including the measure  $dq$ . Notice also that, even once the quorum has been fixed, the unbiased estimator for an operator  $O$  will not in general be unique, since there can exist functions  $\mathcal{N}(Q_\lambda)$  that satisfies

$$\int_A d\lambda \mathcal{N}(Q_\lambda) = 0 , \quad (2.85)$$

and that will be called ‘null estimators’. Two unbiased estimators that differ by a null estimator yield the same results when estimating the operator mean value. We will see in Sect. 2.4.9 how the null estimators can be used to reduce the statistical noise.

In terms of a quorum of observables  $Q_\lambda$  (2.75) rewrites

$$\begin{aligned} \langle O \rangle &= \int_A d\lambda \text{Tr} [OB^\dagger(\lambda)] \text{Tr} [f_\lambda(Q_\lambda)\rho] \\ &= \int_A d\lambda \int dq_\lambda p_\lambda(q_\lambda) \text{Tr} [OB^\dagger(\lambda)] f_\lambda(q_\lambda) , \end{aligned} \quad (2.86)$$

where  $p_\lambda(q_\lambda) = {}_\lambda\langle q|\rho|q\rangle_\lambda$  is the probability density of getting the outcome  $q_\lambda$  from the measurement of  $Q_\lambda$  on the state  $\rho$ . Equation (2.86) is equivalent to the expression (2.62), with the Kernel function

$$\mathcal{R}_\lambda[O](q_\lambda) = \text{Tr} [OB^\dagger(\lambda)] f_\lambda(q_\lambda) . \quad (2.87)$$

Of course it is of interest to connect a quorum of observables to a resolution of the form (2.73), since only in this case can there be a feasible

reconstruction scheme. If a resolution formula is written in terms of a set of selfadjoint operators, the set itself constitutes the desired quorum. However, in general a quorum of observables is functionally connected to the corresponding resolution formula. If the operators  $C(\lambda)$  are unitary, then they can always be considered as exponential of a set of selfadjoint operators, say  $Q_\lambda$ . The quantity  $\text{Tr}[C(\lambda)\rho]$  is thus connected with the moment generating function of the set  $Q_\lambda$ , and hence to the probability density  $p_\lambda(q_\lambda)$  of the measurement outcomes, which play the role of the Radon transform in the quantum tomography of the harmonic oscillator. In general, the operators  $C(\lambda)$  can be any function (neither self-adjoint nor unitary) of observables and, even more generally, they may be connected to POVMs rather than observables.

The dual set  $B(\lambda)$  can be obtained from the set  $C(\lambda)$  by inverting (2.78). For finite quorums, this resorts to a matrix inversion or, alternatively, to a Gram-Schmidt orthogonalization procedure [26]. No such a general procedure exists for a continuous spanning set. Many cases, however, satisfy conditions (2.81) and (2.82), and thus we can write  $B(\lambda) = C^\dagger(\lambda)$ .

### 2.4.5 Quantum Estimation for Harmonic System

The harmonic oscillator models several systems of interest in quantum mechanics, as the vibrational states of molecules, the motion of an ion in a Paul trap, and a single mode radiation field. Different proposals have been suggested in order to reconstruct the quantum state of a harmonic system. They can be summarized using the framework of the previous subsection, which is also useful for devising novel estimation techniques. Here, the basic resolution formula involves the set of displacement operators  $D(\alpha) = \exp(\alpha a^\dagger - \alpha^* a)$ , which can be viewed as exponentials of the field-quadrature operators  $X_\varphi = (a^\dagger e^{i\varphi} + a e^{-i\varphi})/2$ . We have shown in Sect. 2.3.2 that for a single-mode radiation field  $X_\varphi$  is measured through homodyne detection. For the vibrational tomography of a molecule or a trapped ion  $X_\varphi$  corresponds to a time-evolved position or momentum. The set of displacement operators satisfies (2.78) and (2.82), since

$$\text{Tr}[D(\alpha)D^\dagger(\beta)] = \pi\delta^{(2)}(\alpha - \beta), \quad (2.88)$$

whereas (2.83) reduces to the Glauber formula

$$O = \int_{\mathbb{C}} \frac{d^2\alpha}{\pi} \text{Tr}[OD^\dagger(\alpha)] D(\alpha). \quad (2.89)$$

Changing to polar variables  $\alpha = (-i/2)ke^{i\varphi}$ , (2.89) becomes

$$O = \int_0^\pi \frac{d\varphi}{\pi} \int_{-\infty}^{+\infty} \frac{dk|k|}{4} \text{Tr}[O e^{ikX_\varphi}] e^{-ikX_\varphi}, \quad (2.90)$$

which shows explicitly the dependence on the quorum  $X_\varphi$ . Taking the ensemble average of both members and evaluating the trace over the set of eigenvectors of  $X_\varphi$ , one obtains

$$\langle O \rangle = \int_0^\pi \frac{d\varphi}{\pi} \int_{-\infty}^{+\infty} dx p(x, \varphi) \mathcal{R}[O](x, \varphi), \quad (2.91)$$

where  $p(x; \varphi) = {}_\varphi \langle x | \rho | x \rangle_\varphi$  is the probability distribution of quadratures outcome. The Kernel function for the operator  $O$  is given by

$$\mathcal{R}[O](x, \varphi) = \text{Tr}[OK(X_\varphi - x)], \quad (2.92)$$

where  $K(x)$  is the same as in (2.59).

Equation (2.91) is the basis of quantum homodyne tomography. Notice that the operator  $K(x)$  is unbounded, however any matrix element  $\langle \psi | \rho | \phi \rangle$  such that  $\langle \psi | K(X_\varphi - x) | \phi \rangle$  is bounded can be estimated. According to Sect. 2.4.4, the matrix element  $\langle \psi | \rho | \phi \rangle$  can be directly sampled from the homodyne experimental values. In fact, for bounded  $\langle \psi | K(X_\varphi - x) | \phi \rangle$ , the central limit theorem guarantees that

$$\begin{aligned} \langle \psi | \rho | \phi \rangle &= \int_0^\pi \frac{d\varphi}{\pi} \int_{-\infty}^{+\infty} dx p(x, \varphi) \langle \psi | K(X_\varphi - x) | \phi \rangle \\ &= \lim_{N \rightarrow \infty} \frac{1}{N} \sum_{n=0}^N \langle \psi | K(x_{\varphi_n} - x_n) | \phi \rangle, \end{aligned} \quad (2.93)$$

where  $x_n$  is the homodyne outcome measured at phase  $\varphi_n$  and distributed with probability  $p(x, \varphi)$ . Systematic errors are eliminated by choosing randomly each phase  $\varphi_n$  at which homodyne measurement is performed. As shown in Sect. 2.4.4, for finite number of measurements  $N$ , the estimate (2.93) of the integral is Gaussian distributed around the true value  $\langle \psi | \rho | \phi \rangle$ , with statistical error decreasing as  $N^{-1/2}$ . Notice that the measurability of the density operator matrix element depends only on the boundedness of the matrix element of the Kernel function, and that no adjustable parameters are needed in the procedure, which thus is unbiased.

The general procedure for noise deconvolution will be presented in Sect. 2.4.9. However, we give here the main result for the density matrix reconstruction. As shown in Sect. 2.3.2, the effect of the efficiency in homodyne detectors is a Gaussian convolution of the ideal probability  $p(x, \varphi)$ , as

$$p_\eta(x, \varphi) = \sqrt{\frac{2\eta}{\pi(1-\eta)}} \int_{-\infty}^{+\infty} dx' e^{-\frac{2\eta}{1-\eta}(x-x')^2} p(x', \varphi). \quad (2.94)$$

The tomographic reconstruction procedure still holds upon replacing  $p(x, \varphi)$  with  $p_\eta(x, \varphi)$ , so that

$$\rho = \int_0^\pi \frac{d\varphi}{\pi} \int_{-\infty}^{+\infty} dx p_\eta(x, \varphi) K_\eta(X_\varphi - x), \quad (2.95)$$

where now the Kernel function is

$$K_\eta(x) = \frac{1}{2} \text{Re} \int_0^{+\infty} k dk e^{\frac{1-\eta}{8\eta} k^2 + ikx} . \quad (2.96)$$

In fact, by taking the Fourier transform of both members of (2.94), one can easily check that

$$\begin{aligned} \rho &= \int_0^\pi \frac{d\varphi}{\pi} \int_{-\infty}^{+\infty} dx p_\eta(x, \varphi) K_\eta(X_\varphi - x) \\ &= \int_0^\pi \frac{d\varphi}{\pi} \int_{-\infty}^{+\infty} dx p(x, \varphi) K(X_\varphi - x) . \end{aligned} \quad (2.97)$$

Notice that the anti-Gaussian in (2.96) causes a much slower convergence of the Monte Carlo integral (2.95): the statistical fluctuation will increase exponentially for decreasing detector efficiency  $\eta$ . In order to achieve good reconstructions with non-ideal detectors, then one has to collect a larger number of data.

It is clear from (2.93) that the measurability of the density matrix depends on the chosen representation and on the quantum efficiency of the detectors. For example, for the reconstruction of the density matrix in the Fock basis the Kernel functions are given by

$$\begin{aligned} \mathcal{R}_\eta[|n\rangle\langle n+d|](x, \varphi) &= \int_{-\infty}^{+\infty} \frac{dk |k|}{4} e^{\frac{1-\eta}{8\eta} k^2 - ikx} \langle n+d|e^{ikX_\varphi}|n\rangle \quad (2.98) \\ &= e^{id(\varphi + \frac{\pi}{2})} \sqrt{\frac{n!}{(n+d)!}} \int_{-\infty}^{+\infty} dk |k| e^{\frac{1-2\eta}{2\eta} k^2 - i2kx} k^d L_n^d(k^2) , \end{aligned}$$

where  $L_n^d(x)$  denotes the generalized Laguerre polynomials. Notice that the Kernel function is bounded only for  $\eta > 1/2$ , while below this threshold the method would give unbounded statistical errors. However, this bound is well below the values that are reasonably achieved in the lab, where actual homodyne detectors have efficiency ranging between 70% and 90% [11, 68]. The kernel functions for the matrix elements  $\mathcal{R}[|n\rangle\langle n+d|](x, \varphi)$  satisfy the following relation [69, 70, 78]

$$\begin{aligned} \mathcal{R}[|n\rangle\langle n+d|](x, \varphi) &= e^{id\varphi} [4xu_n(x)v_{n+d}(x) \quad (2.99) \\ &\quad - 2\sqrt{n+1}u_{n+1}(x)v_{n+d}(x) - 2\sqrt{n+d+1}u_n(x)v_{n+d+1}(x)] , \quad (2.100) \end{aligned}$$

which can be effectively used to compute the kernel numerically. The functions  $u_j(x)$  and  $v_j(x)$  in (2.100) are the normalizable and unnormalizable eigenfunctions of the harmonic oscillator with eigenvalue  $j$ , respectively. The noise from quantum efficiency can be unbiased via the inversion of the Bernoulli convolution, which holds for  $\eta > 1/2$  [71]. In Fig. 2.3 the  $x$ -dependent part of the Kernel function is reported for different values of  $n$ ,  $d$  and the quantum efficiency  $\eta$ .

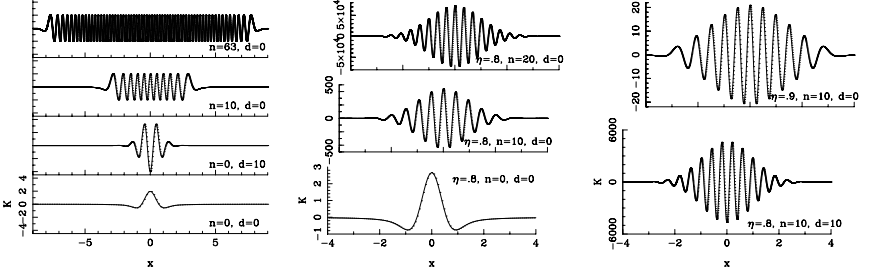


**Fig. 2.3.** The  $x$ -dependent part of the Kernel function  $\mathcal{R}[|n\rangle\langle n+d|](x, \varphi)$  for different values of  $n, d, \eta < 1$ . Notice the very different ranges.

**Table 2.1.** Estimator  $\mathcal{R}_\eta[O](x, \varphi)$  for some operators  $O$  (From [16]).

$O$	$\mathcal{R}_\eta[O](x, \varphi)$
$a^\dagger n a^m$	$e^{i(m-n)\varphi} \frac{H_{n+m}(\sqrt{2\eta}x)}{\sqrt{(2\eta)^{n+m} \binom{n+m}{n}}}$
$a$	$2e^{i\varphi} x$
$a^2$	$e^{2i\varphi} (4x^2 - 1/\eta)$
$a^\dagger a$	$2x^2 - \frac{1}{2\eta}$
$(a^\dagger a)^2$	$\frac{8}{3}x^4 - \frac{4-2\eta}{\eta}x^2 + \frac{1-\eta}{2\eta^2}$
$\hat{W}_s = \frac{2}{\pi(1-s)} \left(\frac{s+1}{s-1}\right) a^\dagger a$	$\int_0^\infty dt \frac{2e^{-t}}{\pi(1-s) - \frac{1}{\eta} \cos\left(2\sqrt{\frac{2t}{(1-s) - \frac{1}{\eta}}x}\right)}$
$ n\rangle\langle n+d $	$\mathcal{R}_\eta[ n\rangle\langle n+d ](x, \varphi)$ in (2.98)

Notice that (2.89) cannot be used for unbounded operators. However, the Kernel functions can be derived also for some unbounded operators, as shown in [16]. In Table 2.1 we report the estimator  $\mathcal{R}_\eta[O](x, \varphi)$  for some operators  $O$ . The operator  $\hat{W}_s$  gives the generalized Wigner function  $W_s(\alpha, \alpha^*)$  for ordering parameter  $s$  through the relation in (2.11). From the expression of  $\mathcal{R}_\eta[\hat{W}_s](x, \varphi)$  it follows that by homodyning with quantum efficiency  $\eta$  one can measure the generalized Wigner function only for  $s < 1 - \eta^{-1}$ : in particular the usual Wigner function for  $s = 0$  cannot be measured for any quantum efficiency.

#### 2.4.6 Some Generalizations

Using condition (2.78) one can see that the Glauber formula can be generalized to

$$O = \int_{\mathbb{C}} \frac{d^2\alpha}{\pi} \text{Tr} [OF_1 D(\alpha) F_2] F_2^{-1} D^\dagger(\alpha) F_1^{-1}, \quad (2.101)$$

where  $F_1$  and  $F_2$  are two generic invertible operators. By choosing  $F_1^\dagger = F_2 =$

$S(\zeta)$ , where  $S(\zeta)$  is the squeezing operator

$$S(\zeta) = \exp \left[ \frac{1}{2} \left( \zeta^2 a^{\dagger 2} - \zeta^{*2} a^2 \right) \right], \quad \zeta \in \mathbb{C}, \quad (2.102)$$

we obtain the tomographic resolution

$$\langle O \rangle = \int_0^\pi \frac{d\varphi}{\pi} \int_{-\infty}^{+\infty} dx p_\zeta(x, \varphi) \text{Tr} [OK(X_{\varphi\zeta} - x)], \quad (2.103)$$

in terms of the probability distribution of the generalized squeezed quadrature operators

$$X_{\varphi\zeta} = S^\dagger(\zeta) X_\varphi S(\zeta) = \frac{1}{2} [(\mu e^{i\varphi} + \nu e^{-i\varphi}) a^\dagger + (\mu e^{-i\varphi} + \nu^* e^{i\varphi}) a], \quad (2.104)$$

with  $\mu = \cosh |\zeta|$  and  $\nu = \sinh |\zeta| \exp(2i \arg[\zeta])$ . Such an estimation technique has been investigated in detail in [72].

A different estimation technique can be obtained by choosing in (2.101)  $F_1 = I$ , the identity operator, and  $F_2 = (-)^{a^\dagger a}$ , the parity operator. In this case one gets

$$O = \int_{\mathbb{C}} \frac{d^2\alpha}{\pi} \text{Tr} [OD^\dagger(\alpha)(-)^{a^\dagger a}] (-)^{a^\dagger a} D(\alpha). \quad (2.105)$$

Changing variable to  $\alpha = 2\beta$  and using the relation

$$(-)^{a^\dagger a} D(2\beta) = D^\dagger(\beta)(-)^{a^\dagger a} D(\beta) \quad (2.106)$$

it follows

$$\langle O \rangle = 4 \int_{\mathbb{C}} \frac{d^2\beta}{\pi} \text{Tr} [OD^\dagger(\beta)(-)^{a^\dagger a} D(\beta)] \text{Tr} [D(\beta)\rho D^\dagger(\beta)(-)^{a^\dagger a}]. \quad (2.107)$$

Hence, it is possible to estimate  $\langle O \rangle$  by repeated measurement of the parity operator on displaced versions of the state under investigation. An approximated implementation of this technique for a single mode radiation field has been suggested in [73, 74] through the measurement of the photon number probability on states displaced by a beam splitter. A similar scheme has been used for the experimental determination of the motional quantum state of a trapped atom [15]. In comparison with the approximated methods, (2.107) allows to directly obtain the Kernel  $\mathcal{R}[O](\alpha)$  for any operator  $O$  for which the trace exists. For instance, the reconstruction of the density matrix in the Fock representation is obtained by averaging the Kernel

$$\begin{aligned} \mathcal{R}[|n\rangle\langle n+d||](\alpha) &= 4\langle n+d|D^\dagger(\alpha)(-)^{a^\dagger a}D(\alpha)|n\rangle \\ &= 4(-)^{n+d} \sqrt{\frac{n!}{(n+d)!}} (2\alpha)^d e^{-2|\alpha|^2} L_n^d(4|\alpha|^2), \end{aligned} \quad (2.108)$$

without the need of artificial cut-off in the Fock space [15].

### 2.4.7 Quantum Estimation for Spin Systems

The so-called spin tomography [20, 30, 66, 67] allows one to reconstruct the quantum state of a spin system from measurements of the spin in different directions, *i.e.* the quorum is the set of operators  $\mathbf{S} \cdot \mathbf{n}$ , where  $\mathbf{S}$  is the spin operator and  $\mathbf{n} \equiv (\cos \varphi \sin \vartheta, \sin \varphi \sin \vartheta, \cos \vartheta)$  is a unit vector. Various different quorums may be constructed by exploiting different sets of directions.

The easiest choice is to consider all possible directions. The procedure to derive the tomographic formulas for this quorum is analogous to the one employed in Sect. 2.4.5 for homodyne tomography. The reconstruction formula for spin tomography for the estimation of an arbitrary operator  $O$  writes

$$\langle O \rangle = \sum_{m=-s}^s \int_{\Omega} \frac{d\mathbf{n}}{4\pi} p(m, \mathbf{n}) \mathcal{R}[O](m, \mathbf{n}), \quad (2.109)$$

where  $p(m, \mathbf{n})$  is the probability of obtaining the eigenvalue  $m$  when measuring the spin along direction  $\mathbf{n}$ ,  $\mathcal{R}[O](m, \mathbf{n})$  is the tomographic Kernel for the operator  $O$ , and  $\Omega$  is the unit sphere. In this case the operators  $C(\lambda)$  of (2.73) are given by the set of projectors over the eigenstates  $|m, \mathbf{n}\rangle$  of the operators  $\mathbf{S} \cdot \mathbf{n}$ . Notice that it is a set of irreducible operators in the system Hilbert space  $\mathcal{H}$ . In order to find the dual basis  $B$ , one must consider the unitary operators obtained by exponentiating the quorum, *i.e.*  $D(\psi, \mathbf{n}) = \exp(i\psi \mathbf{S} \cdot \mathbf{n})$ , which satisfy the bi-orthogonality condition (2.76). In fact,  $D(\psi, \mathbf{n})$  constitutes a unitary irreducible representation of the group  $SU(2)$ , and the bi-orthogonality condition is just the orthogonality relations between the matrix elements of the group representation [75], *i.e.*

$$\int_R dg D_{jr}(g) D_{tk}^\dagger(g) = \frac{V}{d} \delta_{jk} \delta_{tr}, \quad (2.110)$$

where  $D$  is a unitary irreducible representation of dimension  $d$ ,  $dg$  is the group Haar invariant measure, and  $V = \int_R dg$ . For  $SU(2)$ , with the  $2s + 1$  dimension unitary irreducible representation  $D(\psi, \mathbf{n})$ , Haar's invariant measure is  $\sin^2 \frac{\psi}{2} \sin \vartheta d\vartheta d\varphi d\psi$ , and  $\frac{V}{d} = \frac{4\pi^2}{2s+1}$ . The bi-orthogonality condition writes

$$\frac{2s+1}{4\pi^2} \int_{\Omega} d\mathbf{n} \int_0^{2\pi} d\psi \sin^2 \frac{\psi}{2} \langle j | e^{i\psi \mathbf{n} \cdot \mathbf{S}} | r \rangle \langle t | e^{-i\psi \mathbf{n} \cdot \mathbf{S}} | k \rangle = \delta_{jk} \delta_{tr}, \quad (2.111)$$

and hence the spin tomography identity is given by

$$O = \frac{2s+1}{4\pi^2} \int_{\Omega} d\mathbf{n} \int_0^{2\pi} d\psi \sin^2 \frac{\psi}{2} \text{Tr} [OD^\dagger(\psi, \mathbf{n})] D(\psi, \mathbf{n}). \quad (2.112)$$

Notice the analogy between (2.112) and Glauber's formula (2.89). In fact, both homodyne and spin tomography can be derived in the domain of Group

Tomography [20], where the underlying group structure is given by the Weyl-Heisenberg group and the  $SU(2)$  group, respectively. Formula (2.109) is obtained from (2.112) through the expectation value calculated on the eigenstates of  $\mathbf{S} \cdot \mathbf{n}$ . Thus, the explicit form of the tomographic Kernel is obtained as

$$\mathcal{R}[O](m, \mathbf{n}) = \frac{2s+1}{\pi} \int_0^{2\pi} d\psi \sin^2 \frac{\psi}{2} \text{Tr} [O e^{-i\psi \mathbf{S} \cdot \mathbf{n}}] e^{i\psi m} . \quad (2.113)$$

As already noticed, there are other possible quorums for spin tomography. For example, for spin  $s = \frac{1}{2}$  systems, a self-dual basis for the operator space is given by the identity and the Pauli matrices. In fact, from the property  $\sigma_\alpha \sigma_{\alpha'} = \delta_{\alpha\alpha'} I$  ( $\alpha, \alpha' = x, y, z$ ), both the bi-orthogonality relation (2.76) and the trace condition (2.78) follow. In this case the reconstruction formula writes

$$\langle O \rangle = \frac{1}{2} \text{Tr} [O] + \frac{1}{2} \sum_{\alpha=x,y,z} \sum_{m=\pm\frac{1}{2}} m p(m, \mathbf{n}_\alpha) \text{Tr} [O \sigma_\alpha] . \quad (2.114)$$

In the case of generic  $s$  spin system, Weigert has also shown [66] that by choosing  $(2s+1)^2$  arbitrary directions for  $\mathbf{n}$ , it is possible to obtain (in almost all cases) a quorum of projectors  $|s, \mathbf{n}_j\rangle\langle s, \mathbf{n}_j|$  ( $j = 1, \dots, (2s+1)^2$ ), where  $|s, \mathbf{n}_j\rangle$  is the eigenstate pertaining to the maximum eigenvalue  $s$  of  $\mathbf{S} \cdot \mathbf{n}_j$ .

#### 2.4.8 Quantum Estimation for a Free Particle

The state of a moving packet can be inferred from position measurement at different times [76]. Assuming a particle with unit mass and using normalized unit  $\hbar/2 = 1$ , the free Hamiltonian is given by the square of momentum operator  $H_F = p^2$ . In terms of the eigenvectors  $|x\rangle$  of the position operator and of the selfadjoint operator

$$R(x, \tau) = e^{-ip^2\tau} |x\rangle\langle x| e^{ip^2\tau} , \quad (2.115)$$

the probability density of the position of the free particle at time  $\tau$  is obtained as  $p(x, \tau) = \text{Tr}[\rho R(x, \tau)]$ . The operators  $R(x, \tau)$  provide a self-dual basis, and an arbitrary particle state can be written as

$$\rho = \int_{\mathbb{R}} \int_{\mathbb{R}} dx d\tau p(x, \tau) R(x, \tau) . \quad (2.116)$$

#### 2.4.9 Noise Deconvolution and Adaptive Tomography

In the following we will briefly review 1) the noise deconvolution scheme [20, 77], that allows one to eliminate the experimental noise that arises from imperfect detection and lossy devices; 2) the adaptive tomography technique [22] that allows one to tune the unbiased tomographic Kernels to the experimental data one obtains, in order to reduce the statistical noise.

## Noise Deconvolution

Essentially it is possible to eliminate detection noise when it is possible to invert the noise map. A noise process is described by a trace preserving completely positive map  $\Gamma$  acting on the Hilbert space of operators. The noise can be deconvolved at the data analysis if

- the inverse of  $\Gamma$  exists, namely  $\Gamma^{-1} : \mathcal{L}(\mathcal{H}) \rightarrow \mathcal{L}(\mathcal{H})$ , with  $\Gamma^{-1}[\Gamma[O]] = O$ , for  $\forall O \in \mathcal{L}(\mathcal{H})$ .
- the estimator  $\mathcal{E}_\lambda[O](Q_\lambda) = \text{Tr}[O B^\dagger(\lambda)] C(\lambda)$  is in the domain of  $\Gamma^{-1}$
- the map  $\Gamma^{-1}[\mathcal{E}_\lambda[O](Q_\lambda)]$  is a function of  $Q_\lambda$ .

If the above conditions are met, we can recover the “ideal” expectation value  $\langle O \rangle$  that we would get without noise. This is achieved by replacing  $\mathcal{E}_\lambda[O](Q_\lambda)$  with  $\Gamma^{-1}[\mathcal{E}_\lambda[O](Q_\lambda)]$ , and evaluating the ensemble average with the state  $\Gamma^\tau(\rho)$ , namely the state affected by the noise ( $\Gamma^\tau$  represents the dual map, that provides the evolution in the Schroedinger picture). Hence, one has

$$\langle O \rangle = \int_{\Lambda} d\lambda \text{Tr}[\Gamma^{-1}[\mathcal{E}_\lambda[O](Q_\lambda)]\Gamma^\tau(\rho)]. \quad (2.117)$$

Consider for example the noise arising from non-unity quantum efficiency  $\eta$  of homodyne detectors. Recall that the ideal probability density is replaced by a Gaussian convolution with rms  $\Delta_\eta^2 = (1 - \eta)/(4\eta)$ . Then, the map  $\Gamma_\eta$  acts on the quorum as follows

$$\begin{aligned} \Gamma_\eta[e^{ikX_\varphi}] &= \int_{-\infty}^{+\infty} dx e^{ikx} \Gamma_\eta[|x\rangle\langle x|] \\ &= \int_{-\infty}^{+\infty} dx \int_{-\infty}^{+\infty} dx' e^{ikx} e^{-\frac{(x-x')^2}{2\Delta_\eta^2}} [|x'\rangle\langle x'|] = e^{-\frac{1}{2}\Delta_\eta^2 k^2} e^{ikX_\varphi}. \end{aligned} \quad (2.118)$$

Of course one has

$$\Gamma_\eta^{-1}[e^{ikX_\varphi}] = e^{\frac{1}{2}\Delta_\eta^2 k^2} e^{ikX_\varphi}. \quad (2.119)$$

In terms of the Fourier transform of the Kernel function

$$\tilde{\mathcal{R}}[O](y, \varphi) = \int_{-\infty}^{+\infty} \frac{dx}{2\pi} e^{ixy} \mathcal{R}[O](x, \varphi), \quad (2.120)$$

one has

$$\tilde{\mathcal{R}}_\eta[O](y, \varphi) = e^{\frac{1}{2}\Delta_\eta^2 y^2} \tilde{\mathcal{R}}[O](y, \varphi). \quad (2.121)$$

We have implicitly applied the above result in Sect. 2.4.5, where the effect of non-unity quantum efficiency for reconstructing the density matrix elements was discussed. The use of the modified Kernel function in (2.96) and the origin of the bound  $\eta > 1/2$  are indeed due to the invertibility domain of  $\Gamma_\eta$ .

Another simple example of noise deconvolution can be given for a spin  $1/2$  system. Consider the map that describes the “depolarizing channel”

$$\Gamma_p[O] = (1-p)O + \frac{p}{2} \text{Tr}[O] I, \quad 0 \leq p \leq 1. \quad (2.122)$$

This map can be inverted for  $p \neq 1$  as follows

$$\Gamma_p^{-1}[O] = \frac{1}{1-p} \left( O - \frac{p}{2} \text{Tr}[O] I \right). \quad (2.123)$$

Then (2.114) can be replaced with

$$\langle O \rangle = \frac{1}{2} \text{Tr}[O] + \frac{1}{2(1-p)} \sum_{m=\pm\frac{1}{2}} \sum_{\alpha=x,y,z} m p_p(m, \mathbf{n}_\alpha) \text{Tr}[O \sigma_\alpha], \quad (2.124)$$

where now  $p_p(m, \mathbf{n}_\alpha)$  represents the probability of outcome  $m$  when measuring  $\sigma_\alpha$  on the noisy state  $\Gamma_p[\rho]$ .

### Adaptive Tomography

The idea of adaptive tomography is that the tomographic null estimators of (2.85) can be used to reduce the statistical noise arising from the fact that in a real experiment the data sample is always finite. The addition of a null estimator in the ideal case of infinite statistics does not change the measured quantities, since its mean value is zero. In the realistic case of finite statistics, the mean values are statistical variables. As shown in Sect. 2.4.4, by dividing data into statistical blocks and evaluating the tomographic averages, one finds mean values that are Gaussian distributed. Thus, one can look for a procedure to reduce the variance of such distribution. In fact, consider the class of equivalent estimators for  $O$

$$\mathcal{E}'_\lambda[O](Q_\lambda) = \mathcal{E}_\lambda[O](Q_\lambda) + \sum_{i=1}^M \nu_i \mathcal{N}_i(Q_\lambda). \quad (2.125)$$

Each estimator in the class  $\mathcal{E}'$  is identified by the coefficient vector  $\boldsymbol{\nu}$ . The variance of the tomographic averages can be evaluated as

$$\overline{\Delta^2 \mathcal{E}'[O]} = \overline{\Delta^2 \mathcal{E}[O]} + 2 \sum_{i=1}^M \nu_i \overline{\mathcal{N}_i \mathcal{E}[O]} + \sum_{i,j=1}^M \nu_i \nu_j \overline{\mathcal{N}_i \mathcal{N}_j}, \quad (2.126)$$

where  $\overline{F} \equiv \langle \int_{\Lambda} d\lambda F(Q_\lambda) \rangle$ , and

$$\overline{\Delta^2 \mathcal{E}[O]} = \overline{\mathcal{E}^2[O]} - \overline{\mathcal{E}[O]}^2. \quad (2.127)$$

Minimizing  $\overline{\Delta^2 \mathcal{E}'[O]}$  with respect to the coefficients  $\nu_i$ , one obtains the equation

$$\sum_{j=1}^M \nu_j \overline{\mathcal{N}_i \mathcal{N}_j} = -\overline{\mathcal{E}[O] \mathcal{N}_i}, \quad (2.128)$$

which can be solved starting from the estimated mean values, with the vector  $\boldsymbol{\nu}$  as unknown. Notice that the obtained vector  $\boldsymbol{\nu}$  will depend on the experimental data, and has to be calculated with the above procedure for any new set of data.

In summary, the adaptive tomographic algorithm consists in the following steps:

- Find the null estimators  $\mathcal{N}_i(Q_\lambda)$  ( $i = 1, \dots, M$ ) for the quorum which is being used in the experiment.
- Execute the experiment and collect the input data.
- Calculate, using the obtained data, the mean values  $\overline{\mathcal{N}_i \mathcal{N}_j}$  and  $\overline{\mathcal{E}[O] \mathcal{N}_i}$ , and solve the linear system (2.128), to obtain  $\boldsymbol{\nu}$ .
- Use the vector  $\boldsymbol{\nu}$  obtained in the previous step to build the ‘optimized estimator’  $\mathcal{E}'[O](Q_\lambda) = \mathcal{E}[O](Q_\lambda) + \sum_i \nu_i \mathcal{N}_i(Q_\lambda)$ . Using the data collected in the first step, the mean value  $\langle O \rangle$  is now evaluated as

$$\langle O \rangle = \int_{\Lambda} d\lambda \langle \mathcal{E}'_\lambda [O](Q_\lambda) \rangle, \quad (2.129)$$

where the optimized estimator has been used.

- For each new set of data the whole procedure must be repeated, as  $\boldsymbol{\nu}$  is dependent on the data.

Notice that also the mean values are changed in the adaptive tomographic process: null estimators do not change mean values only in the limiting case of infinite statistics. In fact, the mean values are changed in such a way as to reduce the dispersion of the data. Examples of simulations of the adaptive technique that efficiently reduce statistical noise of homodyne tomographic reconstructions can be found in [22]. In homodyne tomography null estimators are obtained as linear combinations of the following functions

$$\mathcal{N}_{k,n}(X_\varphi) = X_\varphi^k e^{\pm i(k+2+2n)\varphi}, \quad k, n \geq 0. \quad (2.130)$$

One can easily check that such functions have zero average over  $\varphi$ , independently on  $\rho$ . Hence, for every operator  $O$  one actually has an equivalence class of infinitely many unbiased estimators, which differ by a linear combination of functions  $\mathcal{N}_{k,n}(X_\varphi)$ . It is then possible to minimize the rms error in the equivalence class by the least-squares method, obtaining in this way an optimal estimator that is *adapted* to the particular set of experimental data.

## 2.5 Multimode Homodyne Tomography

The generalization of homodyne tomography from a single-mode to a multimode field is straightforward, the estimator of simple operator tensors  $O = O_1 \otimes O_2 \otimes \dots \otimes O_n$  being just the product of the estimators of each single-mode operator  $O_1, O_2, \dots, O_n$ . By linearity, one then obtains also the estimator for arbitrary multimode operators. Such a simple generalization, however, requires a separate homodyne detector for each mode, which is unfeasible when the modes of the field are not spatio-temporally separated. This is the case, for example of pulsed fields, for which a general multimode tomographic method is especially needed, also due to the problem of mode matching between the local oscillator and the detected fields (determined by their relative spatio-temporal overlap) [83], which produces a dramatic reduction of the overall quantum efficiency.

In this section we review the general method of [17] for homodyning observables of a multimode electromagnetic field using a *single* local oscillator (LO), providing the rule to evaluate the estimator of an arbitrary multimode operator. The expectation value of the operator can then be obtained by averaging the estimator over the homodyne outcomes that are collected using a single LO whose mode randomly scans all possible linear combinations of incident modes. We will then specifically consider some observables for a two-mode field in a state corresponding to a twin-beam produced by parametric downconversion, and prove the reliability of the method on the basis of computer simulations.

Finally, we report some experimental results [84] obtained in the Prem Kumar's lab at Northwestern University. Such experiment actually represents the first measurement of the joint photon-number probability distribution of the twin-beam state.

### 2.5.1 The General Method

The Hilbert-Schmidt operator expansion in (2.89) can be generalized to any number of modes as follows

$$\begin{aligned}
 O = & \int_{\mathbb{C}} \frac{d^2 z_0}{\pi} \int_{\mathbb{C}} \frac{d^2 z_1}{\pi} \dots \int_{\mathbb{C}} \frac{d^2 z_M}{\pi} \text{Tr} \left\{ O \exp \left[ \sum_{l=0}^M \left( -z_l a_l^\dagger + z_l^* a_l \right) \right] \right\} \\
 & \times \exp \left[ \sum_{l=0}^M \left( z_l a_l^\dagger - z_l^* a_l \right) \right], \quad (2.131)
 \end{aligned}$$

where  $a_l$  and  $a_l^\dagger$ , with  $l = 0, \dots, M$  and  $[a_l, a_{l'}^\dagger] = \delta_{ll'}$ , are the annihilation and creation operators of  $M + 1$  independent modes, and  $O$  now denotes an operator over all modes. Using the following hyper-spherical parameterization

for  $z_l \in \mathbb{C}$

$$z_0 = \frac{i}{2}k u_0(\boldsymbol{\theta})e^{i\psi_0} \doteq \frac{i}{2}k e^{i\psi_0} \cos \theta_1 , \quad (2.132)$$

$$z_1 = \frac{i}{2}k u_1(\boldsymbol{\theta})e^{i\psi_1} \doteq \frac{i}{2}k e^{i\psi_1} \sin \theta_1 \cos \theta_2 ,$$

$$z_2 = \frac{i}{2}k u_2(\boldsymbol{\theta})e^{i\psi_2} \doteq \frac{i}{2}k e^{i\psi_2} \sin \theta_1 \sin \theta_2 \cos \theta_3 ,$$

...

$$z_{M-1} = \frac{i}{2}k u_{M-1}(\boldsymbol{\theta})e^{i\psi_{M-1}} \doteq \frac{i}{2}k e^{i\psi_{M-1}} \sin \theta_1 \sin \theta_2 \dots \sin \theta_{M-1} \cos \theta_M ,$$

$$z_M = \frac{i}{2}k u_M(\boldsymbol{\theta})e^{i\psi_M} \doteq \frac{i}{2}k e^{i\psi_M} \sin \theta_1 \sin \theta_2 \dots \sin \theta_{M-1} \sin \theta_M ,$$

where  $k \in [0, \infty)$ ;  $\psi_l \in [0, 2\pi]$  for  $l = 0, 1, \dots, M$ ; and  $\theta_l \in [0, \pi/2]$  for  $l = 1, 2, \dots, M$ , (2.131) can be rewritten as follows:

$$O = \int d\mu[\boldsymbol{\psi}] \int d\mu[\boldsymbol{\theta}] \int_0^{+\infty} dk \left(\frac{k}{2}\right)^{2M+1} \frac{1}{M!} \\ \times \text{Tr}[O e^{-ikX(\boldsymbol{\theta}, \boldsymbol{\psi})}] e^{ikX(\boldsymbol{\theta}, \boldsymbol{\psi})} . \quad (2.133)$$

Here we have used the notation

$$\int d\mu[\boldsymbol{\psi}] \doteq \prod_{l=0}^M \int_0^{2\pi} \frac{d\psi_l}{2\pi} , \quad (2.134)$$

$$\int d\mu[\boldsymbol{\theta}] \doteq 2^M M! \prod_{l=1}^M \int_0^{\pi/2} d\theta_l \sin^{2(M-l)+1} \theta_l \cos \theta_l , \quad (2.135)$$

$$X(\boldsymbol{\theta}, \boldsymbol{\psi}) = \frac{1}{2} [A^\dagger(\boldsymbol{\theta}, \boldsymbol{\psi}) + A(\boldsymbol{\theta}, \boldsymbol{\psi})] , \quad (2.136)$$

$$A(\boldsymbol{\theta}, \boldsymbol{\psi}) = \sum_{l=0}^M e^{-i\psi_l} u_l(\boldsymbol{\theta}) a_l . \quad (2.137)$$

From the parameterization in (2.133), one has  $\sum_{l=0}^M u_l^2(\boldsymbol{\theta}) = 1$ , and hence  $[A(\boldsymbol{\theta}, \boldsymbol{\psi}), A^\dagger(\boldsymbol{\theta}, \boldsymbol{\psi})] = 1$ , namely  $A(\boldsymbol{\theta}, \boldsymbol{\psi})$  and  $A^\dagger(\boldsymbol{\theta}, \boldsymbol{\psi})$  themselves are annihilation and creation operators of a bosonic mode. By scanning all values of  $\theta_l \in [0, \pi/2]$  and  $\psi_l \in [0, 2\pi]$ , all possible linear combinations of modes  $a_l$  are obtained.

For the quadrature operator  $X(\boldsymbol{\theta}, \boldsymbol{\psi})$  in (2.136), one has the following identity for the moments generating function

$$\langle e^{ikX(\boldsymbol{\theta}, \boldsymbol{\psi})} \rangle = \exp\left(\frac{1-\eta}{8\eta}k^2\right) \int_{-\infty}^{+\infty} dx e^{ikx} p_\eta(x; \boldsymbol{\theta}, \boldsymbol{\psi}) , \quad (2.138)$$

where  $p_\eta(x; \boldsymbol{\theta}, \boldsymbol{\psi})$  denotes the homodyne probability distribution of the quadrature  $X(\boldsymbol{\theta}, \boldsymbol{\psi})$  with quantum efficiency  $\eta$ . Generally,  $\eta$  can depend on

the mode itself, i.e., it is a function  $\eta = \eta(\boldsymbol{\theta}, \boldsymbol{\psi})$  of the selected mode. In the following, for simplicity, we assume  $\eta$  to be mode independent, however. By taking the ensemble average on each side of (2.133) and using (2.138) one has

$$\langle O \rangle = \int d\mu[\boldsymbol{\psi}] \int d\mu[\boldsymbol{\theta}] \int_{-\infty}^{+\infty} dx p_\eta(x; \boldsymbol{\theta}, \boldsymbol{\psi}) \mathcal{R}_\eta[O](x; \boldsymbol{\theta}, \boldsymbol{\psi}), \quad (2.139)$$

where the estimator  $\mathcal{R}_\eta[O](x; \boldsymbol{\theta}, \boldsymbol{\psi})$  has the following expression

$$\begin{aligned} \mathcal{R}_\eta[O](x; \boldsymbol{\theta}, \boldsymbol{\psi}) &= \frac{\kappa^{M+1}}{M!} \int_0^{+\infty} dt e^{-(1-\frac{\kappa}{2})t+2i\sqrt{\kappa t}x} t^M \\ &\times \text{Tr}[O e^{-2i\sqrt{\kappa t}X(\boldsymbol{\theta}, \boldsymbol{\psi})}], \end{aligned} \quad (2.140)$$

with  $\kappa = 2\eta/(2\eta - 1)$ . Equations (2.139) and (2.140) allow one to obtain the expectation value  $\langle O \rangle$  for any unknown state of the radiation field by averaging over the homodyne outcomes of the quadrature  $X(\boldsymbol{\theta}, \boldsymbol{\psi})$  for  $\boldsymbol{\theta}$  and  $\boldsymbol{\psi}$  randomly distributed according to  $d\mu[\boldsymbol{\psi}]$  and  $d\mu[\boldsymbol{\theta}]$ . Such outcomes can be obtained by using a single LO that is prepared in the multimode coherent state  $\otimes_{l=0}^M |\gamma_l\rangle$  with  $\gamma_l = e^{i\psi_l} u_l(\boldsymbol{\theta}) K/2$  and  $K \gg 1$ . In fact, in this case the rescaled zero-frequency photocurrent at the output of a balanced homodyne detector is given by

$$I = \frac{1}{K} \sum_{l=0}^M (\gamma_l^* a_l + \gamma_l a_l^\dagger), \quad (2.141)$$

which corresponds to the operator  $X(\boldsymbol{\theta}, \boldsymbol{\psi})$ . In the limit of a strong LO ( $K \rightarrow \infty$ ), all moments of the current  $I$  correspond to the moments of  $X(\boldsymbol{\theta}, \boldsymbol{\psi})$ , and the exact measurement of  $X(\boldsymbol{\theta}, \boldsymbol{\psi})$  is then realized. Notice that for modes  $a_l$  with different frequencies, in the d.c. photocurrent in (2.141) each LO with amplitude  $\gamma_l$  selects the mode  $a_l$  at the same frequency (and polarization). For less-than-unity quantum efficiency, (2.138) holds.

Equation (2.140) can be applied to some observables of interest. In particular, one can estimate the matrix element  $\langle \{n_l\} | R | \{m_l\} \rangle$  of the multimode density operator  $R$ . This will be obtained by averaging the estimator

$$\begin{aligned} \mathcal{R}_\eta[\{m_l\} \langle \{n_l\} \rangle](x; \boldsymbol{\theta}, \boldsymbol{\psi}) &= e^{-i \sum_{l=0}^M (n_l - m_l) \psi_l} \frac{\kappa^{M+1}}{M!} \\ &\times \prod_{l=0}^M \left\{ [-i\sqrt{\kappa} u_l(\boldsymbol{\theta})]^{\mu_l - \nu_l} \sqrt{\frac{\nu_l!}{\mu_l!}} \right\} \\ &\times \int_0^{+\infty} dt e^{-t+2i\sqrt{\kappa t}x} t^{M+\sum_{l=0}^M (\mu_l - \nu_l)/2} \prod_{l=0}^M L_{\nu_l}^{\mu_l - \nu_l}[\kappa u_l^2(\boldsymbol{\theta})t], \end{aligned} \quad (2.142)$$

where  $\mu_l = \max(m_l, n_l)$ ,  $\nu_l = \min(m_l, n_l)$ , and  $L_n^\alpha(z)$  denotes the generalized Laguerre polynomial. For diagonal matrix elements, (2.142) simplifies to

$$\begin{aligned} \mathcal{R}_\eta[|\{n_l\}\rangle\langle\{n_l\}|](x; \boldsymbol{\theta}, \boldsymbol{\psi}) = \\ \frac{\kappa^{M+1}}{M!} \int_0^{+\infty} dt e^{-t+2i\sqrt{\kappa t}x} t^M \prod_{l=0}^M L_{n_l}[\kappa u_l^2(\boldsymbol{\theta})t] \end{aligned} \quad (2.143)$$

with  $L_n(z)$  denoting the customary Laguerre polynomial in  $z$ . Using the following identity [79]

$$\begin{aligned} L_n^{\alpha_0+\alpha_1+\dots+\alpha_M+M}(x_0+x_1+\dots+x_M) \\ = \sum_{i_0+i_1+\dots+i_M=n} L_{i_0}^{\alpha_0}(x_0)L_{i_1}^{\alpha_1}(x_1)\dots L_{i_M}^{\alpha_M}(x_M), \end{aligned} \quad (2.144)$$

from (2.143) one can easily derive the estimator of the probability distribution of the total number of photons  $N = \sum_{l=0}^M a_l^\dagger a_l$

$$\mathcal{R}_\eta[|n\rangle\langle n|](x; \boldsymbol{\theta}, \boldsymbol{\psi}) = \frac{\kappa^{M+1}}{M!} \int_0^{+\infty} dt e^{-t+2i\sqrt{\kappa t}x} t^M L_n^M[\kappa t], \quad (2.145)$$

where  $|n\rangle$  denotes the eigenvector of  $N$  with eigenvalue  $n$ . Notice that the estimator in (2.143) does not depend on the phases  $\psi_l$ ; only the knowledge of the angles  $\theta_l$  is needed. For the estimator in (2.145), even the angles  $\theta_l$  can be unknown.

Now we specialize to the case of only two modes  $a$  and  $b$  (i.e.,  $M=1$  and  $\boldsymbol{\theta}$  is a scalar  $\theta$ ). The joint photon-number probability distribution is obtained by averaging

$$\begin{aligned} \mathcal{R}_\eta[|n, m\rangle\langle n, m|](x; \theta, \psi_0, \psi_1) = \\ \kappa^2 \int_0^{+\infty} dt e^{-t+2i\sqrt{\kappa t}x} t L_n(\kappa t \cos^2 \theta) L_m(\kappa t \sin^2 \theta). \end{aligned} \quad (2.146)$$

The estimator (2.145) of the probability distribution of the total number of photons can be written as

$$\mathcal{R}_\eta[|n\rangle\langle n|](x; \theta, \psi_0, \psi_1) = \kappa^2 \int_0^{+\infty} dt e^{-t+2i\sqrt{\kappa t}x} t L_n^1[\kappa t]. \quad (2.147)$$

For the total number of photons one can also derive the estimator of the moment generating function, using the generating function for the Laguerre polynomials [79]. One obtains

$$\mathcal{R}_\eta[z^{a^\dagger a + b^\dagger b}](x; \theta, \psi_0, \psi_1) = \frac{1}{(z + \frac{1-z}{\kappa})^2} \Phi\left(2, \frac{1}{2}; -\frac{1-z}{z + \frac{1-z}{\kappa}} x^2\right). \quad (2.148)$$

For the first two moments one obtains the simple expressions

$$\begin{aligned}\mathcal{R}_\eta[a^\dagger a + b^\dagger b](x; \theta, \psi_0, \psi_1) &= 4x^2 + \frac{2}{\kappa} - 2, \\ \mathcal{R}_\eta[(a^\dagger a + b^\dagger b)^2](x; \theta, \psi_0, \psi_1) &= 8x^4 + \left(\frac{24}{\gamma} - 20\right)x^2 + \frac{6}{\gamma^2} - \frac{10}{\gamma} + 4.\end{aligned}\quad (2.149)$$

It is worth noting that analogous estimators of the photon-number difference between the two modes are singular and one needs a cutoff procedure, similar to the one used in [85] for recovering the correlation between the modes by means of the customary two-mode tomography. In fact, in order to extract information pertaining to a single mode only one needs a delta-function at  $\theta = 0$  for mode  $a$ , or  $\theta = \pi/2$  for mode  $b$ , and, in this case, one could better use the standard one-mode tomography by setting the LO to the proper mode of interest.

Finally, we note that for two-mode tomography the estimators can be averaged by the integral

$$\begin{aligned}\langle O \rangle &= \int_0^{2\pi} \frac{d\psi_0}{2\pi} \int_0^{2\pi} \frac{d\psi_1}{2\pi} \int_{-1}^1 \frac{d(\cos 2\theta)}{2} \int_{-\infty}^{+\infty} dx p_\eta(x; \theta, \psi_0, \psi_1) \\ &\times \mathcal{R}_\eta[O](x; \theta, \psi_0, \psi_1)\end{aligned}\quad (2.150)$$

over the random parameters  $\cos(2\theta)$ ,  $\psi_0$ , and  $\psi_1$ . For example, in the case of two radiation modes having the same frequency but orthogonal polarizations,  $\theta$  represents a random rotation of the polarizations, whereas  $\psi_0$  and  $\psi_1$  denote the relative phases between the LO and the two modes, respectively.

### 2.5.2 Numerical Results for Two-Mode Fields

In this section we report some Monte-Carlo simulations from [17] to judge the experimental working conditions for performing the single-LO tomography on two-mode fields. We focus our attention on the twin-beam state, usually generated by spontaneous parametric downconversion, namely

$$|\Psi\rangle = S(\chi)|0\rangle_a|0\rangle_b = \sqrt{1 - |\xi|^2} \sum_{n=0}^{\infty} \xi^n |n\rangle_a |n\rangle_b, \quad (2.151)$$

where  $S(\chi) = \exp(\chi a^\dagger b^\dagger - \chi^* ab)$  and  $\xi = e^{i \arg \chi} \tanh|\chi|$ . The parameter  $\xi$  is related to the average number of photons per beam  $\bar{n} = |\xi|^2/(1 - |\xi|^2)$ . For the simulations we need to derive the homodyne probability distribution  $p(x; \theta, \psi_0, \psi_1)$  which is given by

$$\begin{aligned}p(x; \theta, \psi_0, \psi_1) &= \text{Tr}[U^\dagger |x\rangle_{aa}\langle x| \otimes 1_b U |\Psi\rangle\langle\Psi|] \\ &= {}_a\langle 0|_b\langle 0| S^\dagger(\chi) U^\dagger [|x\rangle_{aa}\langle x| \otimes 1_b] U S(\chi) |0\rangle_a|0\rangle_b,\end{aligned}\quad (2.152)$$

where  $|x\rangle_a$  is the eigenvector of the quadrature  $x = \frac{1}{2}(a^\dagger + a)$  with eigenvalue  $x$  and  $U$  is the unitary operator achieving the mode transformation

$$U^\dagger \begin{pmatrix} a \\ b \end{pmatrix} U = \begin{pmatrix} e^{-i\psi_0} \cos \theta & e^{-i\psi_1} \sin \theta \\ -e^{i\psi_1} \sin \theta & e^{i\psi_0} \cos \theta \end{pmatrix} \begin{pmatrix} a \\ b \end{pmatrix}. \quad (2.153)$$

In the case of two radiation modes having the same frequency but orthogonal polarizations—the case of Type II phase-matched parametric amplifier—(2.152) gives the theoretical probability of outcome  $x$  for the homodyne measurement at a polarization angle  $\theta$  with respect to the polarization of the  $a$  mode, and with  $\psi_0$  and  $\psi_1$  denoting the relative phases between the LO and the two modes, respectively. The probability in (2.152) is given by [17]

$$p(x; \theta, \psi_0, \psi_1) \frac{1}{\sqrt{2\pi\Delta^2(\theta, \psi_0, \psi_1)}} \exp\left(-\frac{x^2}{2\Delta^2(\theta, \psi_0, \psi_1)}\right), \quad (2.154)$$

where the variance  $\Delta^2(\theta, \psi_0, \psi_1)$  reads

$$\Delta^2(\theta, \psi_0, \psi_1) = \frac{1 + |\xi|^2 + 2|\xi| \sin 2\theta \cos(\psi_0 + \psi_1 - \arg \xi)}{4(1 - |\xi|^2)}. \quad (2.155)$$

Taking into account the Gaussian convolution that results from less-than-unity quantum efficiency, the variance just increases as

$$\Delta^2(\theta, \psi_0, \psi_1) \rightarrow \Delta_\eta^2(\theta, \psi_0, \psi_1) = \Delta^2(\theta, \psi_0, \psi_1) + \frac{1 - \eta}{4\eta}. \quad (2.156)$$

Notice that the probability distribution in (2.154) corresponds to a squeezed vacuum for  $\theta = \frac{\pi}{4}$  and  $\psi_0 + \psi_1 - \arg \xi = 0$  or  $\pi$ .

We study the tomographic measurement of the joint photon-number probability distribution and the probability distribution for the total number of photons with use of the estimators in (2.146) and (2.147), respectively. The estimators have been numerically evaluated by applying the Gauss method for calculating the integral in (2.142), which results in a fast and sufficiently precise algorithm with use of just 150 evaluation points.

In Fig. 2.4 a Monte-Carlo simulation of the joint photon-number probability distribution is reported. The simulated values compare very well with the theoretical ones. In [17] a careful analysis of the statistical errors has been done for various twin-beam states by constructing histograms of deviations of the results from different simulated experiments from the theoretical ones. In comparison to the customary two-LO tomography of [85], where for  $\eta = 1$  the statistical errors saturate for increasingly large  $n$  and  $m$ , here we have statistical errors that are slowly increasing versus  $n$  and  $m$ . This is due to the fact that the range of the estimators in (2.146) increases versus  $n$  and  $m$ . Overall we find that for any given quantum efficiency the statistical errors are generally slightly larger than those obtained with the two-LO method. The convenience of using a single LO then comes with its own price tag.

By using the estimator in (2.147) the probability distribution for the total number of photons  $N$  of the twin beams has been also constructed (Fig. 2.5). Notice the dramatic increase of error bars versus  $N$  and for smaller  $\eta$ .

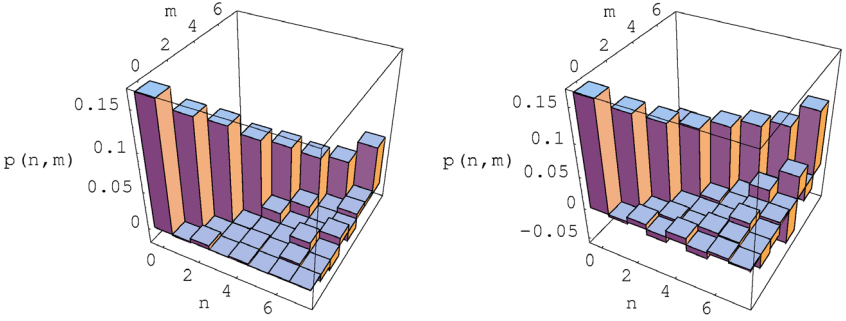


**Fig. 2.4.** Two-mode photon-number probability  $p(n, m)$  of the twin-beam state in (2.151) for average number of photons per beam  $\bar{n} = 5$  obtained by a Monte-Carlo simulation with the estimator in (2.146) and random parameters  $\cos 2\theta$ ,  $\psi_0$ , and  $\psi_1$ . On the left: quantum efficiency  $\eta = 1$  and  $10^6$  data samples were used in the reconstruction. On the right:  $\eta = 0.9$ , and  $5 \times 10^6$  data samples (From [17]).

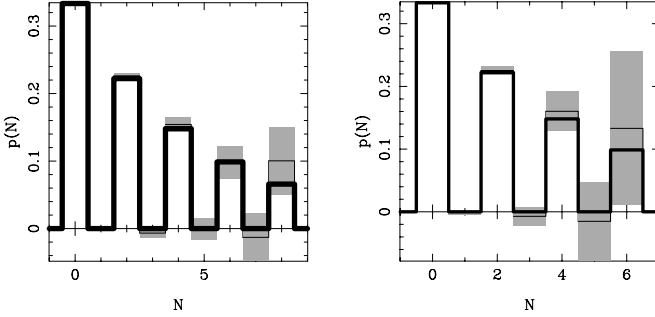


**Fig. 2.5.** Probability distribution for the total number of photons of the twin beams in (2.151) for average number of photons per beam  $\bar{n} = 2$  obtained using the estimator in (2.147). Samples of  $10^7$  data with quantum efficiency  $\eta = 0.9$  (on the left), and of  $2 \times 10^7$  data with  $\eta = 0.8$  (on the right). The theoretical probability (thick solid line) is superimposed onto the result of the Monte-Carlo experiment; the latter is shown by the thin solid line. Notice the dramatic increase of errors (in gray shade) versus  $N$  and for smaller  $\eta$  (From [17]).

The first experimental results of a measurement of the joint photon-number probability distribution for a two-mode quantum state created by a nondegenerate optical parametric amplifier has been presented in [84]. In this experiment, however, the twin beams are detected separately by two balanced-homodyne detectors. Some experimental results are reported in Fig. 2.6. As expected for parametric fluorescence, the experiment has shown a measured joint photon-number probability distribution that exhibited up to 1.9 dB of quantum correlation between the two modes, with thermal marginal distributions.

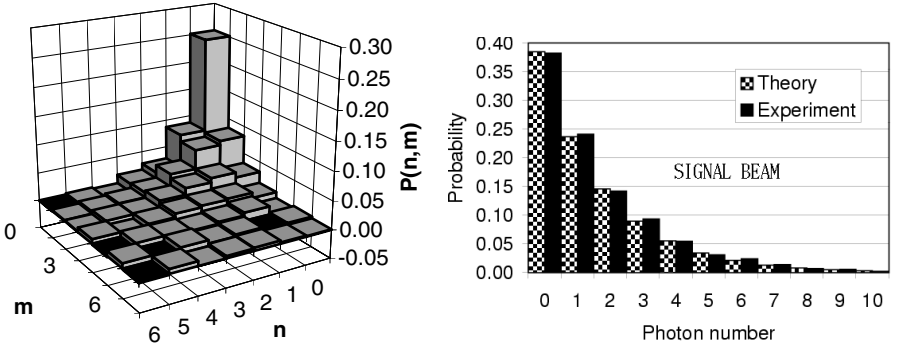


**Fig. 2.6.** Left: Measured joint photon-number probability distribution for the twin-beam state with average number of photons per beam  $\bar{n} = 1.5$  and 400000 samples. Right: marginal distribution for the signal beam for the same data. The theoretical distribution is also shown. Very similar results are obtained for the idler beam (From [84]).

## 2.6 Maximum-Likelihood Method in Quantum Estimation

Quantum estimation of states, observables and parameters is, from very basic principles, matter of statistical inference from a population sampling, and the most comprehensive quantum estimation procedure is quantum tomography. As we have shown in Sect. 3, the expectation value of an operator is obtained by averaging an estimator over the experimental data of a “quorum” of observables. The method is very general and efficient, however, in the averaging procedure, we have fluctuations which result in relatively large statistical errors.

Another relevant strategy, the maximum-likelihood (ML) method, can be used in quantum estimation. The ML strategy [86,87] is an entirely different approach to quantum state measurement compared to the standard quantum-tomographic techniques. The ML procedure consists in finding the quantum state, or the value of the parameters, that are most likely to generate the observed data. This idea can be quantified and implemented using the concept of the likelihood functional.

A detailed account of ML methods in quantum estimation will be given in the chapter by Z. Hradil *et al* in this book. Here we will review the applications of ML proposed in [23] and [31] to the quantum state reconstruction, with examples for both radiation and spin systems, and, finally, considering the ML estimation for the relevant class of Gaussian states in quantum optics.

As regards state estimation, the ML method estimates the quantum state as a whole. Such a procedure incorporates *a priori* knowledge about relations between elements of the density matrix. This guarantees positivity and normalization of matrix, with the result of a substantial reduction of statis-

tical errors. Regarding the estimation of specific parameters, we notice that in many cases the resulting estimators are efficient, unbiased and consistent, thus providing a statistically reliable determination.

As we will show, by using the ML method only small samples of data are required for a precise determination. However, ML may not always be the optimal solution of the tomographic problem. Besides being biased due to the Hilbert space truncation—even though the bias can be very small if, from other methods, we know where to truncate—it cannot be generalized to the estimation of any ensemble average, but just of a set of parameters from which the density matrix depends. In addition, for increasing number of parameters the method has exponential complexity.

### 2.6.1 Maximum Likelihood Principle

Here we briefly review the theory of the maximum-likelihood (ML) estimation of a single parameter. The generalization to several parameters, as for example the elements of the density matrix, is straightforward. The only point that should be carefully analyzed is the parameterization of the multidimensional quantity to be estimated. In the next section the specific case of the density matrix will be discussed.

Let  $p(x|\lambda)$  the probability density of a random variable  $x$ , conditioned to the value of the parameter  $\lambda$ . The form of  $p$  is known, but the true value of  $\lambda$  is unknown, and will be estimated from the result of a measurement of  $x$ . Let  $x_1, x_2, \dots, x_N$  be a random sample of size  $N$ . The joint probability density of the independent random variable  $x_1, x_2, \dots, x_N$  (the global probability of the sample) is given by

$$\mathcal{L}(x_1, x_2, \dots, x_N|\lambda) = \prod_{k=1}^N p(x_k|\lambda), \quad (2.157)$$

and is called the likelihood function of the given data sample (hereafter we will suppress the dependence of  $\mathcal{L}$  on the data). The maximum-likelihood estimator (MLE) of the parameter  $\lambda$  is defined as the quantity  $\lambda_{ml} \equiv \lambda_{ml}(\{x_k\})$  that maximizes  $\mathcal{L}(\lambda)$  for variations of  $\lambda$ , namely  $\lambda_{ml}$  is given by the solution of the equations

$$\frac{\partial \mathcal{L}(\lambda)}{\partial \lambda} = 0; \quad \frac{\partial^2 \mathcal{L}(\lambda)}{\partial \lambda^2} < 0. \quad (2.158)$$

The first equation is equivalent to  $\partial L/\partial \lambda = 0$  where

$$L(\lambda) = \log \mathcal{L}(\lambda) = \sum_{k=1}^N \log p(x_k|\lambda) \quad (2.159)$$

is the so-called log-likelihood function.

In order to obtain a measure for the confidence interval in the determination of  $\lambda_{ml}$  we consider the variance

$$\sigma_\lambda^2 = \int \left[ \prod_k dx_k p(x_k|\lambda) \right] [\lambda_{ml}(\{x_k\}) - \lambda]^2 . \quad (2.160)$$

In terms of the Fisher information

$$F = \int dx \left[ \frac{\partial p(x|\lambda)}{\partial \lambda} \right]^2 \frac{1}{p(x|\lambda)} , \quad (2.161)$$

it is easy to prove that

$$\sigma_\lambda^2 \geq \frac{1}{NF} , \quad (2.162)$$

where  $N$  is the number of measurements. The inequality in (2.162) is known as the Cramér-Rao bound [88] on the precision of the ML estimation. Notice that this bound holds for any functional form of the probability distribution  $p(x|\lambda)$ , provided that the Fisher information exists  $\forall \lambda$  and  $\partial_\lambda p(x|\lambda)$  exists  $\forall x$ . When an experiment has “good statistics” (i.e. for a large enough data sample) the Cramér-Rao bound is saturated.

## 2.6.2 ML Quantum State Estimation

In this section we review the method of the maximum likelihood estimation of the quantum state of [23], focusing attention to the cases of homodyne and spin tomography.

We consider an experiment consisting of  $N$  measurements performed on identically prepared copies of a given quantum system. Each measurement is described by a positive operator-valued measure (POVM). The outcome of the  $i$ th measurement corresponds to the realization of a specific element of the POVM used in the corresponding run, and we denote this element by  $\Pi_i$ . The likelihood is here a functional of the density matrix  $\mathcal{L}(\rho)$  and is given by the product

$$\mathcal{L}(\rho) = \prod_{i=1}^N \text{Tr}(\rho \Pi_i) , \quad (2.163)$$

which represents the probability of the observed data. The unknown element of the above expression, which we want to infer from data, is the density matrix describing the measured ensemble. The estimation strategy of the ML technique is to maximize the likelihood functional over the set of the density matrices. Several properties of the likelihood functional are easily found, if we restrict ourselves to finite dimensional Hilbert spaces. In this case, it can be easily proved that  $\mathcal{L}(\rho)$  is a concave function defined on a convex and closed

set of density matrices. Therefore, its maximum is achieved either on a single isolated point, or on a convex subset of density matrices. In the latter case, the experimental data are insufficient to provide a unique estimate for the density matrix using the ML strategy. On the other hand, the existence of a single maximum allows us to assign unambiguously the ML estimate for the density matrix.

The ML estimation of the quantum state, despite its elegant general formulation, results in a highly nontrivial constrained optimization problem, even if we resort to purely numerical means. The main difficulty lies in the appropriate parameterization of the set of all density matrices. The parameter space should be of the minimum dimension in order to preserve the maximum of the likelihood function as a single isolated point. Additionally, the expression of quantum expectation values in terms of this parameterization should enable fast evaluation of the likelihood function, as this step is performed many times in the course of numerical maximization.

For such purpose one introduces [23] a parameterization of the set of density matrices which provides an efficient algorithm for maximization of the likelihood function. We represent the density matrix in the form

$$\rho = T^\dagger T, \quad (2.164)$$

which automatically guarantees that  $\rho$  is positive and Hermitian. The remaining condition of unit trace  $\text{Tr}\rho = 1$  will be taken into account using the method of Lagrange multipliers. In order to achieve the minimal parameterization, we assume that  $T$  is a complex lower triangular matrix, with real elements on the diagonal. This form of  $T$  is motivated by the Cholesky decomposition known in numerical analysis [89] for arbitrary non negative Hermitian matrix. For an  $M$ -dimensional Hilbert space, the number of real parameters in the matrix  $T$  is  $M + 2M(M - 1)/2 = M^2$ , which equals the number of independent real parameters for a Hermitian matrix. This confirms that such parameterization is minimal, up to the unit trace condition.

In numerical calculations, it is convenient to replace the likelihood functional by its natural logarithm, which of course does not change the location of the maximum. Thus the log-likelihood function subjected to numerical maximization is given by

$$L(T) = \sum_{i=1}^N \ln \text{Tr}(T^\dagger T \Pi_i) - \lambda \text{Tr}(T^\dagger T), \quad (2.165)$$

where  $\lambda$  is a Lagrange multiplier accounting for normalization of  $\rho$ . Writing  $\rho$  in terms of its eigenvectors  $|\psi_\mu\rangle$  as  $\rho = \sum_\mu y_\mu^2 |\psi_\mu\rangle\langle\psi_\mu|$ , with real  $y_\mu$ , the maximum likelihood condition  $\partial L/\partial y_\nu = 0$  reads

$$\lambda y_\nu = \sum_{i=1}^N [y_\nu \langle\psi_\nu|\Pi_i|\psi_\nu\rangle / \text{Tr}(\rho \Pi_i)], \quad (2.166)$$

which, after multiplication by  $y_\nu$  and summation over  $\nu$ , yields  $\lambda = N$ . The Lagrange multiplier then equals the total number of measurements  $N$ .

This formulation of the maximization problem allows one to apply standard numerical procedures for searching the maximum over the  $M^2$  real parameters of the matrix  $T$ . The examples presented below use the downhill simplex method [90].

The first example is the ML estimation of a single-mode radiation field. The experimental apparatus used in this technique is the homodyne detector. According to Sect. 2.3.3 the homodyne measurement is described by the positive operator-valued measure

$$\mathcal{H}(x; \varphi) = \sqrt{\frac{2\eta}{\pi(1-\eta)}} \exp\left[-\frac{2\eta}{1-\eta}(X_\varphi - x)^2\right], \quad (2.167)$$

where  $\eta$  is the detector efficiency, and  $X_\varphi = (a^\dagger e^{i\varphi} + a e^{-i\varphi})/2$  is the quadrature operator at phase  $\varphi$ .

After  $N$  measurements, we obtain a set of pairs  $(x_i; \varphi_i)$ , where  $i = 1, \dots, N$ . The log-likelihood functional is given by (2.165) with  $\Pi_i \equiv \mathcal{H}(x_i; \varphi_i)$ . Of course, for a light mode it is necessary to truncate the Hilbert space to a finite dimensional basis. We shall assume that the highest Fock state has  $M - 1$  photons, i.e. that the dimension of the truncated Hilbert space is  $M$ . For the expectation  $\text{Tr}[T^\dagger T \mathcal{H}(x; \varphi)]$  it is necessary to use an expression which is explicitly positive, in order to protect the algorithm against occurrence of small negative numerical arguments of the logarithm function. A simple derivation yields

$$\text{Tr}[T^\dagger T \mathcal{H}(x; \varphi)] = \sqrt{\eta} \sum_{k=0}^{M-1} \sum_{j=0}^k \left| \sum_{n=0}^{k-j} \langle k|T|n+j\rangle B_{n+j,n} \langle n|\sqrt{\eta}x\rangle e^{in\varphi} \right|^2, \quad (2.168)$$

where

$$B_{n+j,n} = \left[ \binom{n+j}{n} \eta^n (1-\eta)^j \right]^{1/2}, \quad (2.169)$$

and

$$\langle n|x\rangle = \left(\frac{2}{\pi}\right)^{1/4} \frac{1}{\sqrt{2^n n!}} H_n(\sqrt{2}x) \exp(-x^2) \quad (2.170)$$

are the eigenstates of the harmonic oscillator in the position representation— $H_n(x)$  being the  $n$ th Hermite polynomial.

The ML technique can be applied to reconstruct the density matrix in the Fock basis from Monte Carlo simulated homodyne statistics. Figure 2.7 depicts the matrix elements of the density operator as obtained for a co-

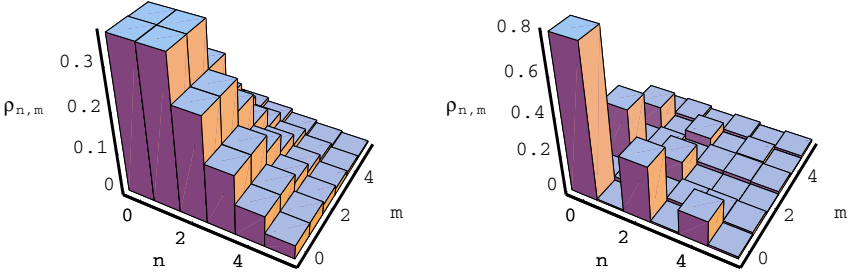


**Fig. 2.7.** Reconstruction of the density matrix of a single-mode radiation field by the ML method. The plot shows the matrix elements of a coherent state (left) with  $\langle a^\dagger a \rangle = 1$  photon, and for a squeezed vacuum (right) with  $\langle a^\dagger a \rangle = 0.5$  photon. A sample of 50000 simulated homodyne data for quantum efficiency  $\eta = 80\%$  has been used (From [23]).

herent state and a squeezed vacuum, respectively. Remarkably, only 50000 homodyne data have been used for quantum efficiency  $\eta = 80\%$ . We recall that in quantum homodyne tomography the statistical errors are known to grow rapidly with decreasing efficiency  $\eta$  of the detector [78, 91]. In contrast, the elements of the density matrix reconstructed using the ML approach remain bounded, as the whole matrix must satisfy positivity and normalization constraints. This results in much smaller statistical errors. As a comparison one could see that the same precision of the reconstructions in Fig. 2.7 could be achieved using  $10^7$ – $10^8$  data samples with conventional quantum tomography. On the other hand, in order to find numerically the ML estimate we need to set *a priori* the cut-off parameter for the photon number, and its value is limited by increasing computation time.

Another relevant example is the reconstruction of the quantum state of two-mode field using single-LO homodyning. Here, the full joint density matrix can be measured by scanning the quadratures of all possible linear combinations of modes. For two modes the measured quadrature operator is given by

$$X(\theta, \psi_0, \psi_1) = \frac{1}{2}(ae^{-i\psi_0} \cos \theta + be^{-i\psi_1} \sin \theta + \text{h.c.}), \quad (2.171)$$

where  $(\theta, \psi_0, \psi_1) \in S^2 \times [0, 2\pi]$ ,  $S^2$  being the Poincaré sphere and one phase ranging between 0 and  $2\pi$ . In each run these parameters are chosen randomly. The POVM describing the measurement is given by the right-hand side of (2.167), with  $X_\varphi$  replaced by  $X(\theta, \psi_0, \psi_1)$ . An experiment for the two orthogonal states  $|\Psi_1\rangle = (|00\rangle + |11\rangle)/\sqrt{2}$  and  $|\Psi_2\rangle = (|01\rangle + |10\rangle)/\sqrt{2}$  has been simulated, in order to reconstruct the density matrix in the two-mode Fock basis using the ML technique. The results are reported in Fig. 2.8.

The ML procedure can also be applied for reconstructing the density matrix of spin systems. For example, let us consider  $N$  repeated preparations of a pair of spin-1/2 particles. The particles are shared by two parties. In

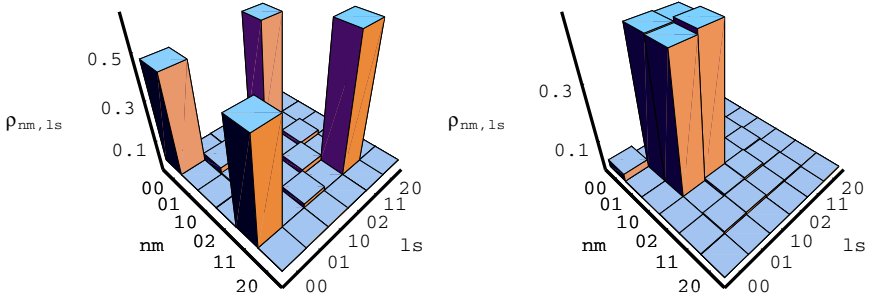


**Fig. 2.8.** ML reconstruction of the density matrix of a two-mode radiation field. On the left the matrix elements obtained for the state  $|\Psi_1\rangle = (|00\rangle + |11\rangle)/\sqrt{2}$ ; on the right for  $|\Psi_2\rangle = (|01\rangle + |10\rangle)/\sqrt{2}$ . For  $|\Psi_1\rangle$  we used 100000 simulated homodyne data and  $\eta = 80\%$ ; for  $|\Psi_2\rangle$  we used 20000 data and  $\eta = 90\%$  (From [23]).

each run, the parties select randomly and independently from each other a direction along which they perform a spin measurement. The obtained result is described by the joint projection operator (spin coherent states [92])  $\mathcal{F}_i = |\Omega_i^A, \Omega_i^B\rangle\langle\Omega_i^A, \Omega_i^B|$ , where  $\Omega_i^A$  and  $\Omega_i^B$  are the vectors on the Bloch sphere corresponding to the outcomes of the  $i$ th run, and the indices  $A$  and  $B$  refer to the two particles. As in the previous examples, it is convenient to use an expression for the quantum expectation value  $\text{Tr}(T^\dagger T \mathcal{F}_i)$  which is explicitly positive. The suitable form is

$$\text{Tr}(T^\dagger T \mathcal{F}_i) = \sum_{\mu} |\langle\mu|T|\Omega_i^A, \Omega_i^B\rangle|^2, \quad (2.172)$$

where  $|\mu\rangle$  is an orthonormal basis in the Hilbert space of the two particles.

Summarizing, the ML technique can be used to estimate the density matrix of a quantum system. With respect to conventional quantum tomography this method has the great advantage of needing much smaller experimental samples, making experiments with low data rates feasible, however with a truncation of the Hilbert space dimension. We have shown that the method is general and the algorithm has solid methodological background, its reliability being confirmed in a number of Monte Carlo simulations. However, for increasing dimension of Hilbert spaces the method has exponential complexity.

### 2.6.3 Gaussian-State Estimation

In this section we review the ML determination method of [31] for the parameters of Gaussian states. Such states represent the wide class of coherent, squeezed and thermal states, all of them being characterized by a Gaussian Wigner function. Apart from an irrelevant phase, we consider Wigner functions of the form

$$W(x, y) = \frac{2\Delta^2}{\pi} \exp\{-2\Delta^2 [e^{-2r}(x - \text{Re}\mu)^2 + e^{2r}(y - \text{Im}\mu)^2]\}, \quad (2.173)$$

and the ML technique with homodyne detection is applied to estimate the four real parameters  $\Delta, r, \text{Re}\mu$  and  $\text{Im}\mu$ . The four parameters provide the number of thermal, squeezing and coherent-signal photons in the quantum state as follows

$$\begin{aligned} n_{th} &= \frac{1}{2} \left( \frac{1}{\Delta^2} - 1 \right), \\ n_{sq} &= \sinh^2 r, \\ n_{coh} &= |\mu|^2. \end{aligned} \quad (2.174)$$

The density matrix  $\rho$  corresponding to the Wigner function in (2.173) writes

$$\rho = D(\mu) S(r) \frac{1}{n_{th} + 1} \left( \frac{n_{th}}{n_{th} + 1} \right)^{a^\dagger a} S^\dagger(r) D^\dagger(\mu), \quad (2.175)$$

where  $S(r) = \exp[r(a^2 - a^{\dagger 2})/2]$  and  $D(\mu) = \exp(\mu a^\dagger - \mu^* a)$  denote the squeezing and displacement operators, respectively.

The theoretical homodyne probability distribution at phase  $\varphi$  with respect to the local oscillator can be evaluated using (2.7), and is given by the Gaussian

$$\begin{aligned} p(x, \varphi) &= \sqrt{\frac{2\Delta^2}{\pi(e^{2r} \cos^2 \varphi + e^{-2r} \sin^2 \varphi)}} \\ &\times \exp \left\{ -\frac{2\Delta^2}{e^{2r} \cos^2 \varphi + e^{-2r} \sin^2 \varphi} [x - \text{Re}(\mu e^{-i\varphi})]^2 \right\}. \end{aligned} \quad (2.176)$$

The log-likelihood function (2.159) for a set of  $N$  homodyne outcomes  $x_i$  at random phase  $\varphi_i$  then writes as follows

$$\begin{aligned} L &= \sum_{i=1}^N \frac{1}{2} \log \frac{2\Delta^2}{\pi(e^{2r} \cos^2 \varphi_i + e^{-2r} \sin^2 \varphi_i)} \\ &\quad - \frac{2\Delta^2}{e^{2r} \cos^2 \varphi_i + e^{-2r} \sin^2 \varphi_i} [x_i - \text{Re}(\mu e^{-i\varphi_i})]^2. \end{aligned} \quad (2.177)$$

The ML estimators  $\Delta_{ml}, r_{ml}, \text{Re}\mu_{ml}$  and  $\text{Im}\mu_{ml}$  are found upon maximizing (2.177) versus  $\Delta, r, \text{Re}\mu$  and  $\text{Im}\mu$ .

In order to evaluate globally the state reconstruction, one considers the normalized overlap  $\mathcal{O}$  between the theoretical and the estimated state

$$\mathcal{O} = \frac{\text{Tr}[\rho \rho_{ml}]}{\sqrt{\text{Tr}[\rho^2] \text{Tr}[\rho_{ml}^2]}}. \quad (2.178)$$

Notice that  $\mathcal{O} = 1$  iff  $\rho = \rho_{ml}$ . Through Monte-Carlo simulations, one always finds a value around unity, typically with statistical fluctuations over the third digit, for number of data samples  $N = 50000$ , quantum efficiency

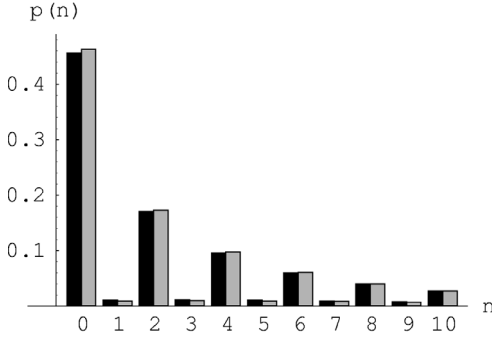


**Fig. 2.9.** Photon-number probability of a squeezed-thermal state (thermal photons  $n_{th} = 0.1$ , squeezing photons  $n_{sq} = 3$ ). Compare the reconstructed probabilities by means of the maximum likelihood method and homodyne detection (gray histogram) with the theoretical values (black histogram). Number of data samples  $N = 50000$ , quantum efficiency  $\eta = 80\%$ . The statistical error affects the third decimal digit, and it is not visible on the scale of the plot (From [31]).

at homodyne detectors  $\eta = 80\%$ , and state parameters with the following ranges:  $n_{th} < 3$ ,  $n_{coh} < 5$ , and  $n_{sq} < 3$ . Also with such a small number of data samples, the quality of the state reconstruction is so good that other physical quantities that are theoretically evaluated from the experimental values of  $\Delta_{ml}$ ,  $r_{ml}$ ,  $\text{Re}\mu_{ml}$  and  $\text{Im}\mu_{ml}$  are inferred very precisely. For example, in [31] the photon number probability of a squeezed thermal state has been evaluated, which is given by the integral

$$\langle n | \rho | n \rangle = \int_0^{2\pi} \frac{d\phi}{2\pi} \frac{[C(\phi, n_{th}, r) - 1]^n}{C(\phi, n_{th}, r)^{n+1}}, \quad (2.179)$$

with  $C(\phi, n_{th}, r) = (n_{th} + \frac{1}{2})(e^{-2r} \sin^2 \phi + e^{2r} \cos^2 \phi) + \frac{1}{2}$ . The comparison of the theoretical and the experimental results for a state with  $n_{th} = 0.1$  and  $n_{sq} = 3$  is reported in Fig. 2.9. The statistical error of the reconstructed number probability affects the third decimal digit, and is not visible on the scale of the plot.

The estimation of parameters of Gaussian Wigner functions through the ML method allows one to estimate the parameters in quadratic Hamiltonians of the generic form

$$H = \alpha a + \alpha^* a^\dagger + \varphi a^\dagger a + \frac{1}{2} \xi a^2 + \frac{1}{2} \xi^* a^{\dagger 2}. \quad (2.180)$$

In fact, the unitary evolution operator  $U = e^{-iHt}$  preserves the Gaussian form of an input state with Gaussian Wigner function. In other words, one can use a known Gaussian state to probe and characterize an optical device described by a Hamiltonian as in (2.180). Assuming  $t = 1$  without loss of

generality, the Heisenberg evolution of the radiation mode  $a$  is given by

$$U^\dagger a U = \gamma a + \delta a^\dagger + \mu, \quad (2.181)$$

with

$$\gamma = \cos(\sqrt{\varphi^2 - |\xi|^2}) - i \frac{\varphi}{\sqrt{\varphi^2 - |\xi|^2}} \sin(\sqrt{\varphi^2 - |\xi|^2}), \quad (2.182)$$

$$\delta = -i \frac{\xi^*}{\sqrt{\varphi^2 - |\xi|^2}} \sin(\sqrt{\varphi^2 - |\xi|^2}),$$

$$\mu = \frac{\varphi \alpha^* - \xi^* \alpha}{\varphi^2 - |\xi|^2} (\cos(\sqrt{\varphi^2 - |\xi|^2}) - 1) - i \frac{\alpha^*}{\sqrt{\varphi^2 - |\xi|^2}} \sin(\sqrt{\varphi^2 - |\xi|^2}).$$

For an input state  $\rho$  with known Wigner function  $W_\rho(\beta, \beta^*)$ , the corresponding output Wigner function writes

$$W_{U\rho U^\dagger}(\beta, \beta^*) = W_\rho[(\beta - \mu)\gamma^* - (\beta^* - \mu^*)\delta, (\beta^* - \mu^*)\gamma - (\beta - \mu)\delta^*]. \quad (2.183)$$

Hence, by estimating the parameters  $\gamma, \delta, \mu$  and inverting (2.182), one obtains the ML values for  $\alpha, \varphi$ , and  $\xi$  of the Hamiltonian in (2.180). The present example can be used in practical applications for the estimation of the gain of a phase-sensitive amplifier or equivalently to estimate a squeezing parameter.

## Acknowledgments

This work has been co-sponsored by: the Italian *Ministero dell'Istruzione, dell'Università e della Ricerca* (MIUR) under the Cofinanziamento 2003 *New generation of quantum measuring devices for photon quantum information technology*, the *Istituto Nazionale di Fisica della Materia* under the project PRA-2002-CLON, and by the European Community program ATE-SIT (Contract No. IST-2000-29681). M. G. A. P. is research fellow at *Collegio Alessandro Volta*.

## References

1. W. Heisenberg: *Zeit. für Physik* **43**, 172 (1927); W. Heisenberg: *The physical principle of Quantum Theory* (Univ. Chicago Press, Dover, NY, 1930).
2. J. von Neumann: *Mathematical Foundations of Quantum Mechanics* (Princeton Univ. Press, NJ, 1955).
3. W. K. Wootters and W. H. Zurek: *Nature* **299**, 802 (1982); H. P. Yuen: *Phys. Lett. A* **113**, 405 (1986).
4. G. M. D'Ariano and H. P. Yuen: *Phys. Rev. Lett.* **76**, 2832 (1996).
5. U. Fano: *Rev. Mod. Phys.* **29**, 74 (1957), Sec. 6.

6. D. T. Smithey, M. Beck, M. G. Raymer, and A. Faridani: Phys. Rev. Lett. **70**, 1244 (1993); M. G. Raymer, M. Beck, and D. F. McAlister: Phys. Rev. Lett. **72**, 1137 (1994); D. T. Smithey, M. Beck, J. Cooper, and M. G. Raymer: Phys. Rev. A **48**, 3159 (1993).
7. K. Vogel and H. Risken: Phys. Rev. A **40**, 2847 (1989).
8. G. M. D'Ariano, C. Macchiavello and M. G. A. Paris: Phys. Rev. A **50**, 4298 (1994).
9. G. M. D'Ariano, U. Leonhardt and H. Paul: Phys. Rev. A **52**, R1801 (1995).
10. M. Munroe, D. Boggavarapu, M. E. Anderson, M. G. Raymer: Phys. Rev. A **52**, R924 (1995).
11. S. Schiller, G. Breitenbach, S. F. Pereira, T. M. Huller, J. Mlynek: Phys. Rev. Lett. **77**, 2933 (1996); G. Breitenbach, S. Schiller, and J. Mlynek: Nature **387**, 471 (1997).
12. U. Janicke and M. Wilkens: J. Mod. Opt. **42**, 2183 (1995); S. Wallentowitz and W. Vogel: Phys. Rev. Lett. **75**, 2932 (1995); S. H. Kienle, M. Freiberger, W. P. Schleich, and M. G. Raymer: In *Experimental Metaphysics: Quantum Mechanical Studies for Abner Shimony*, ed by Cohen S. et al. (Kluwer, Lancaster, 1997) p. 121.
13. T. J. Dunn, I. A. Walmsley, and S. Mukamel: Phys. Rev. Lett. **74**, 884 (1995).
14. C. Kurtsiefer, T. Pfau, and J. Mlynek: Nature **386**, 150 (1997).
15. D. Leibfried, D. M. Meekhof, B. E. King, C. Monroe, W. M. Itano, and D. J. Wineland: Phys. Rev. Lett. **77**, 4281 (1996).
16. G. M. D'Ariano: In *Quantum Communication, Computing, and Measurement*, ed by O. Hirota, A. S. Holevo and C. M. Caves (Plenum Publishing, New York and London, 1997) p. 253.
17. G. M. D'Ariano, P. Kumar, and M. F. Sacchi: Phys. Rev. A **61**, 013806 (2000).
18. G. M. D'Ariano: In *Quantum Communication, Computing, and Measurement*, ed by Kumar P., D'Ariano G. M. Hirota O. (Kluwer Academic/Plenum Publishers, New York and London, 2000) p. 137.
19. M. Painsi: preprint quant-ph/0002078.
20. G. M. D'Ariano: Phys. Lett. A **268**, 151 (2000).
21. G. Cassinelli, G. M. D'Ariano, E. De Vito, and A. Levrero: J. Math. Phys. **41**, 7940 (2000).
22. G. M. D'Ariano and M. G. A. Paris: Acta Phys. Slov. **48**, 191 (1998); Phys. Rev. A **60**, 518 (1999).
23. K. Banaszek, G. M. D'Ariano, M. G. A. Paris, and M. F. Sacchi: Phys. Rev. A **61**, R010304 (2000).
24. G. M. D'Ariano, P. Kumar, and M. F. Sacchi: Phys. Rev. A **59**, 826 (1999).
25. G. M. D'Ariano, P. Kumar, C. Macchiavello, L. Maccone, and N. Sterpi: Phys. Rev. Lett. **83**, 2490 (1999).
26. G. M. D'Ariano, L. Maccone and M. G. A. Paris: Phys. Lett. A **276**, 25 (2000); J. Phys. A **34**, 93 (2001).
27. G. M. D'Ariano and P. Lo Presti: Phys. Rev. Lett. **86**, 4195 (2001).
28. E. P. Wigner: Phys. Rev. **40**, 749 (1932).
29. K. E. Cahill and R. J. Glauber: Phys. Rev. **177**, 1857 (1969); Phys. Rev. **177**, 1882 (1969).
30. G. M. D'Ariano, L. Maccone, and M. Painsi: J. Opt. B **5**, 77 (2003).
31. G. M. D'Ariano, M. G. A. Paris and M. F. Sacchi: Phys. Rev. A **62**, 023815 (2000); Phys. Rev. A **64**, 019903(E) (2001).

32. G. M. D'Ariano and M. F. Sacchi: *Nuovo Cimento* **112B**, 881 (1997).
33. *The Physics of Phase Space*, ed by Y. S. Kim and W. W. Zachary (Springer, Berlin, 1986).
34. C. W. Gardiner: *Quantum noise* (Springer-Verlag, Berlin, 1991).
35. H. Weyl: *The Theory of Groups and Quantum Mechanics* (Dover, New York, 1950).
36. K. E. Cahill: *Phys. Rev.* **138**, B1566 (1965).
37. G. M. D'Ariano, M. Fortunato and P. Tombesi: *Nuovo Cimento* **110B**, 1127 (1995).
38. C. T. Lee: *Phys. Rev. A* **44**, R2775 (1991); *Phys. Rev. A* **52**, 3374 (1995).
39. P. L. Kelley and W. H. Kleiner: *Phys. Rev.* **136**, 316 (1964).
40. H. P. Yuen and V. W. S. Chan: *Opt. Lett.* **8**, 177 (1983).
41. G. L. Abbas, V. W. S. Chan, S. T. Yee: *Opt. Lett.* **8**, 419 (1983); *IEEE J. Light. Tech.* **LT-3**, 1110 (1985).
42. G. M. D'Ariano: *Nuovo Cimento* **107B**, 643 (1992).
43. G. M. D'Ariano: Quantum estimation theory and optical detection. In: *Quantum Optics and the Spectroscopy of Solids*, ed by T. Hakioglu and A. S. Shumovsky (Kluwer, Dordrecht, 1997) pp. 139-174.
44. K. Wodkiewicz and J. H. Eberly: *JOSA B* **2**, 458 (1985).
45. G. M. D'Ariano: *Int. J. Mod. Phys. B* **6**, 1291 (1992).
46. H. P. Yuen and J. H. Shapiro: *IEEE Trans. Inf. Theory* **24**, 657 (1978); **25**, 179 (1979).
47. H. P. Yuen and J. H. Shapiro: *IEEE Trans. Inf. Theory* **26**, 78 (1980).
48. G. M. D'Ariano, P. Lo Presti and M. F. Sacchi: *Phys. Lett. A* **272**, 32 (2000).
49. G. M. D'Ariano and M. F. Sacchi: *Phys. Rev. A* **52**, R4309 (1995).
50. C. W. Helstrom: *Quantum Detection and Estimation Theory* (Academic Press, New York, 1976).
51. E. Arthurs and J. L. Kelly, Jr.: *Bell System Tech. J.* **44**, 725 (1965).
52. H. P. Yuen: *Phys. Lett.* **91A**, 101 (1982).
53. E. Arthurs and M. S. Goodman: *Phys. Rev. Lett.* **60**, 2447 (1988).
54. G. M. D'Ariano, C. Macchiavello, and M. G. A. Paris: *Phys. Lett. A* **198**, 286 (1995).
55. M. G. A. Paris: *Phys. Rev. A* **53**, 2658 (1996).
56. R. Baltin: *J. Phys. A* **16**, 2721 (1983); *Phys. Lett. A* **102**, 332 (1984).
57. M. G. A. Paris: *Opt. Comm.* **124**, 277 (1996).
58. J. H. Shapiro and S. S. Wagner: *IEEE J. Quant. Electron.* **QE-20**, 803 (1984).
59. J. H. Shapiro: *IEEE J. Quant. Electron.* **QE-21**, 237 (1985).
60. N. G. Walker: *J. Mod. Opt.* **34**, 15 (1987).
61. Y. Lai and H. A. Haus: *Quantum Opt.* **1**, 99 (1989).
62. M. G. A. Paris, A. Chizhov, and O. Steuernagel: *Opt. Comm.* **134**, 117 (1986).
63. A. Zucchetti, W. Vogel, and D. G. Welsch: *Phys. Rev. A* **54**, 856 (1996).
64. G. M. D'Ariano: *Phys. Lett. A* **300**, 1 (2002).
65. T. Opatrny and D. -G. Welsch: In *Prog. Opt.*, vol. XXXIX, ed by E. Wolf (Elsevier, Amsterdam, 1999) p. 63.
66. S. Weigert: *Phys. Rev. Lett.* **84**, 802 (2000).
67. H. F. Hofmann, S. Takeuchi: preprint quant-ph/0310003.
68. C. Kim and P. Kumar: *Phys. Rev. Lett.* **73**, 1605 (1994).
69. Th. Richter: *Phys. Lett. A* **211**, 327 (1996).
70. U. Leonhardt, M. Munroe, T. Kiss, M. G. Raymer, and Th. Richter: *Opt. Comm.* **127**, 144 (1996).

71. T. Kiss, U. Herzog, and U. Leonhardt: Phys. Rev. A **52**, 2433 (1995); G. M. D'Ariano and C. Macchiavello: Phys. Rev. A **57**, 3131 (1998); T. Kiss, U. Herzog, and U. Leonhardt: Phys. Rev. A **57**, 3131 (1998).
72. G. M. D'Ariano, S. Mancini, V. I. Manko, and P. Tombesi: Q. Opt. **8**, 1017 (1996).
73. K. Banaszek and K. Wodkiewicz: Phys. Rev. Lett. **76**, 4344 (1996).
74. T. Opatrny and D. -G. Welsch: Phys. Rev. A **55**, 1462 (1997).
75. F. D. Murnaghan: *The theory of group representation* (Johns Hopkins Press, 1938), p. 216.
76. U. Leonhardt and M. G. Raymer: Phys. Rev. Lett. **76**, 1985 (1996).
77. G. M. D'Ariano: Acta Phys. Slov. **49**, 513 (1999).
78. G. M. D'Ariano, C. Macchiavello, and N. Sterpi: Quantum Semiclass Opt. **9**, 929 (1997).
79. I. S. Gradshteyn and I. M. Ryzhik: *Table of integrals, series, and products* (Academic Press, New York, 1980).
80. Th. Richter: Phys. Rev. A **53**, 1197 (1996).
81. A. Orłowski, A. Wünsche: Phys. Rev. A **48**, 4617 (1993).
82. A. S. Holevo: *Probabilistic and Statistical Aspects of Quantum Theory* (North-Holland Publishing, Amsterdam, 1982).
83. J. H. Shapiro and A. Shakeel: JOSA B **14**, 232 (1997).
84. M. Vasilyev, S.-K. Choi, P. Kumar, and G. M. D'Ariano: Phys. Rev. Lett. **84**, 2354 (2000).
85. G. M. D'Ariano, M. Vasilyev, and P. Kumar: Phys. Rev. A **58**, 636 (1998).
86. Z. Hradil: Phys. Rev. A **55**, R1561 (1997); in the context of phase measurement, see S. L. Braunstein, A. S. Lane, and C. M. Caves: Phys. Rev. Lett. **69**, 2153 (1992).
87. K. Banaszek: Phys. Rev. A **57**, 5013 (1998).
88. H. Cramer: *Mathematical Methods of Statistics* (Princeton University Press, Princeton, 1946).
89. A. S. Householder: *The Theory of Matrices in Numerical Analysis* (Blaisdell, New York, 1964) Sec. 5.2.
90. W. H. Press, S. A. Teukolsky, W. T. Vetterling, and B. P. Flannery: *Numerical Recipes in Fortran* (Cambridge Univ. Press, Cambridge, 1992) Sec. 10.4.
91. G. M. D'Ariano and M. G. A. Paris: Phys. Lett. A **233**, 49 (1997).
92. F. T. Arecchi, E. Courtens, R. Gilmore, and H. Thomas: Phys. Rev. A **6**, 2211 (1972).
93. F. Natterer: *The mathematics of computerized tomography* (Wiley, New York, 1986).
94. P. Mansfield and P. G. Morris: *NMR Imaging in Biomedicine* (Academic Press, New York, 1982).